Pro-inflammatory Aorta-Associated Macrophages Are Involved in Embryonic Development of Hematopoietic Stem Cells

Mariani, Samanta Antonella ; Li, Zhuan ; Rice, Siobhan ; Krieg, Carsten ; Fragkogianni, Stamatina ; Robinson, Mark D ; Vink, Chris Sebastiaan ; Pollard, Jeffrey William ; Dzierzak, Elaine

Abstract: Hematopoietic stem cells (HSCs) are generated from specialized endothelial cells of the embryonic aorta. Inflammatory factors are implicated in regulating mouse HSC development, but which cells in the aorta-gonad-mesonephros (AGM) microenvironment produce these factors is unknown. In the adult, macrophages play both pro- and anti-inflammatory roles. We sought to examine whether macrophages or other hematopoietic cells found in the embryo prior to HSC generation were involved in the AGM HSC-generative microenvironment. CyTOF analysis of $CD45^{+}$ AGM cells revealed predominance of two hematopoietic cell types, mannose-receptor positive macrophages and mannose-receptor negative myeloid cells. We show here that macrophage appearance in the AGM was dependent on the chemokine receptor Cx3cr1. These macrophages expressed a pro-inflammatory signature, localized to the aorta, and dynamically interacted with nascent and emerging intra-aortic hematopoietic cells (IAHCs). Importantly, upon macrophage depletion, no adult-repopulating HSCs were detected, thus implicating a role for pro-inflammatory AGM-associated macrophages in regulating the development of HSCs.

DOI: https://doi.org/10.1016/j.immuni.2019.05.003

Article

Immunity

Pro-inflammatory Aorta-Associated Macrophages Are Involved in Embryonic Development of Hematopoietic Stem Cells

Graphical Abstract

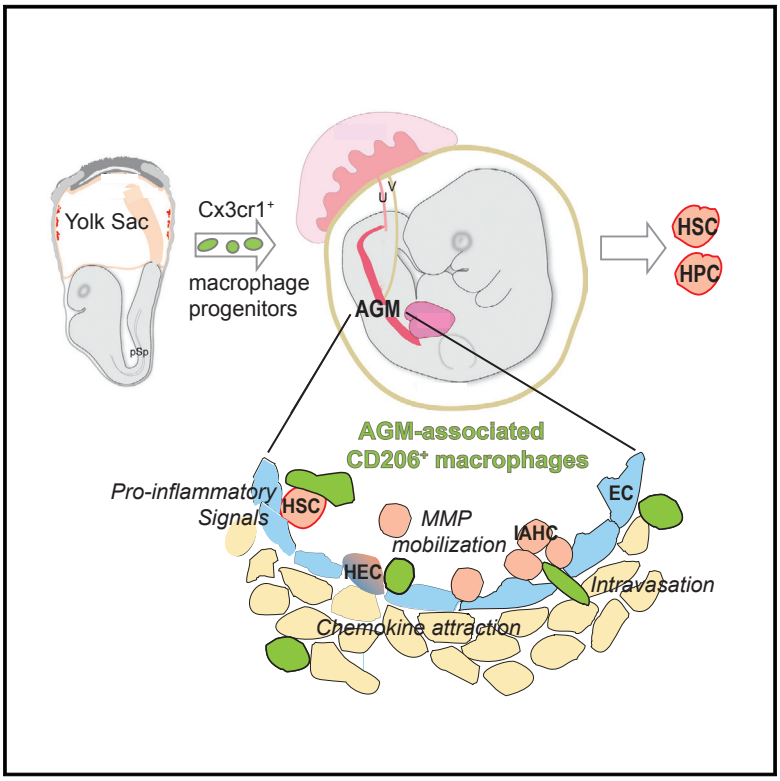

Authors

Samanta Antonella Mariani, Zhuan Li, Siobhan Rice, ..., Chris Sebastiaan Vink, Jeffrey William Pollard, Elaine Dzierzak

Correspondence

s.mariani@ed.ac.uk (S.A.M.), elaine.dzierzak@ed.ac.uk (E.D.)

In Brief

HSC-independent macrophages derive from the early yolk-sac stages of embryonic hematogenesis. Mariani and colleagues demonstrate that specific pro-inflammatory embryonic HSC-independent macrophages recruited to the AGM (AGM-aMs) are crucial components of the AGM microenvironment, dynamically interact with emerging hematopoietic cells, and enhance HSC generation.

Highlights

- Yolk-sac-derived macrophages are the most abundant hematopoietic cells in the AGM
- Cx3cr1 mediates yolk-sac macrophage progenitor recruitment to the AGM niche
- AGM macrophages dynamically interact with emerging intra-aortic hematopoietic cells
- Pro-inflammatory AGM macrophages are positive regulators of HSC generation

Mariani et al., 2019, Immunity *50*, 1439–1452
June 18, 2019
https://doi.org/10.1016/j.immuni.2019.05.003

CellPress

Immunity
Article

Pro-inflammatory Aorta-Associated Macrophages Are Involved in Embryonic Development of Hematopoietic Stem Cells

Samanta Antonella Mariani,[1,*] Zhuan Li,[1] Siobhan Rice,[1] Carsten Krieg,[2] Stamatina Fragkogianni,[4] Mark Robinson,[3] Chris Sebastiaan Vink,[1] Jeffrey William Pollard,[4] and Elaine Dzierzak[1,5,*]
[1]Centre for Inflammation Research, The University of Edinburgh, Edinburgh, UK
[2]Medical University of South Carolina, Charleston, SC, USA
[3]University of Zurich, Zurich, Switzerland
[4]MRC Centre for Reproductive Health, The University of Edinburgh, Edinburgh, UK
[5]Lead Contact
*Correspondence: s.mariani@ed.ac.uk (S.A.M.), elaine.dzierzak@ed.ac.uk (E.D.)
https://doi.org/10.1016/j.immuni.2019.05.003

SUMMARY

Hematopoietic stem cells (HSCs) are generated from specialized endothelial cells of the embryonic aorta. Inflammatory factors are implicated in regulating mouse HSC development, but which cells in the aorta-gonad-mesonephros (AGM) microenvironment produce these factors is unknown. In the adult, macrophages play both pro- and anti-inflammatory roles. We sought to examine whether macrophages or other hematopoietic cells found in the embryo prior to HSC generation were involved in the AGM HSC-generative microenvironment. CyTOF analysis of CD45$^+$ AGM cells revealed predominance of two hematopoietic cell types, mannose-receptor positive macrophages and mannose-receptor negative myeloid cells. We show here that macrophage appearance in the AGM was dependent on the chemokine receptor Cx3cr1. These macrophages expressed a pro-inflammatory signature, localized to the aorta, and dynamically interacted with nascent and emerging intra-aortic hematopoietic cells (IAHCs). Importantly, upon macrophage depletion, no adult-repopulating HSCs were detected, thus implicating a role for pro-inflammatory AGM-associated macrophages in regulating the development of HSCs.

INTRODUCTION

Hematopoietic stem cell (HSC) transplantation is a curative regenerative therapy for patients with blood-related disorders. More than 50,000 transplants are carried out annually worldwide. For patients without a histo-compatible donor, the lack of matched HSCs is a serious problem. Given that HSCs do not expand in *in vitro* cultures, patient-derived induced pluripotent stem cells (iPSCs) may be an alternative source for the *de novo* production of HSCs. Although it is possible to differentiate iPSCs and to reprogram cells into hematopoietic progenitors, the generation of robust *in vivo* repopulating HSCs *in vitro* has not yet been achieved without genetic manipulation (Doulatov et al., 2013). Thus, an understanding of the *in vivo* microenvironment in which HSCs are first generated should provide insights into improving such *in vitro* strategies.

HSCs arise in the AGM (aorta-gonad-mesonephros) region (Medvinsky and Dzierzak, 1996) and other major arteries (de Bruijn et al., 2000) through a transdifferentiation process called endothelial-to-hematopoietic transition (EHT) (Dzierzak and Bigas, 2018; Jaffredo et al., 1998). In the mouse embryo, HSCs are generated in a complex and dynamic microenvironment during a short period of developmental time (embryonic day [E] 10.5–E12.5) (Zovein et al., 2008). Tissues ventral to the AGM (Peeters et al., 2009; Taoudi and Medvinsky, 2007), including cells of the sympathetic nervous system (Fitch et al., 2012), exert a positive effect on HSC emergence. Moreover, AGM-derived stromal cell lines produce regulators, such as bone morphogenetic protein (BMP) and hedgehog (Hh), that support HSC generation and/or maintenance, as demonstrated by transcriptional profiling and culture approaches (Charbord et al., 2014; Crisan et al., 2015; Durand et al., 2007; Renström et al., 2009).

Hematopoietic development occurs in at least three distinct waves (Dzierzak and Bigas, 2018), with HSCs made only in the last wave. Macrophages are generated in all three waves, first in the mouse yolk sac (YS) beginning at E7.5 (Palis et al., 1999; Tober et al., 2007), then in the second YS wave at E8.25 (Gomez Perdiguero et al., 2015) from erythro-myeloid progenitors (EMPs) (Frame et al., 2013; Palis et al., 1999), and finally from HSC-derived monocytes. EMPs emigrate to the embryo body, where they give rise to hematopoietic cells found in the embryo prior to HSC emergence at E10.5. Because the three distinct waves of hematopoietic generation temporally overlap, the hematopoietic cells generated in the earlier two waves could be part of the microenvironment that affects the production of HSCs intraembryonically in the third wave (Chen et al., 2011; Espín-Palazón et al., 2014; Li et al., 2014; Travnickova et al., 2015).

Macrophages from the first two waves function developmentally in tissue remodeling (Hume et al., 1983; Leid et al., 2016; Munro et al., 2019). They infiltrate the limbs, mandibular arches, liver, kidneys, and brain between E9.5 and E10.5 and represent 2%–5% of total cells in these tissues (Rae et al., 2007). In adult

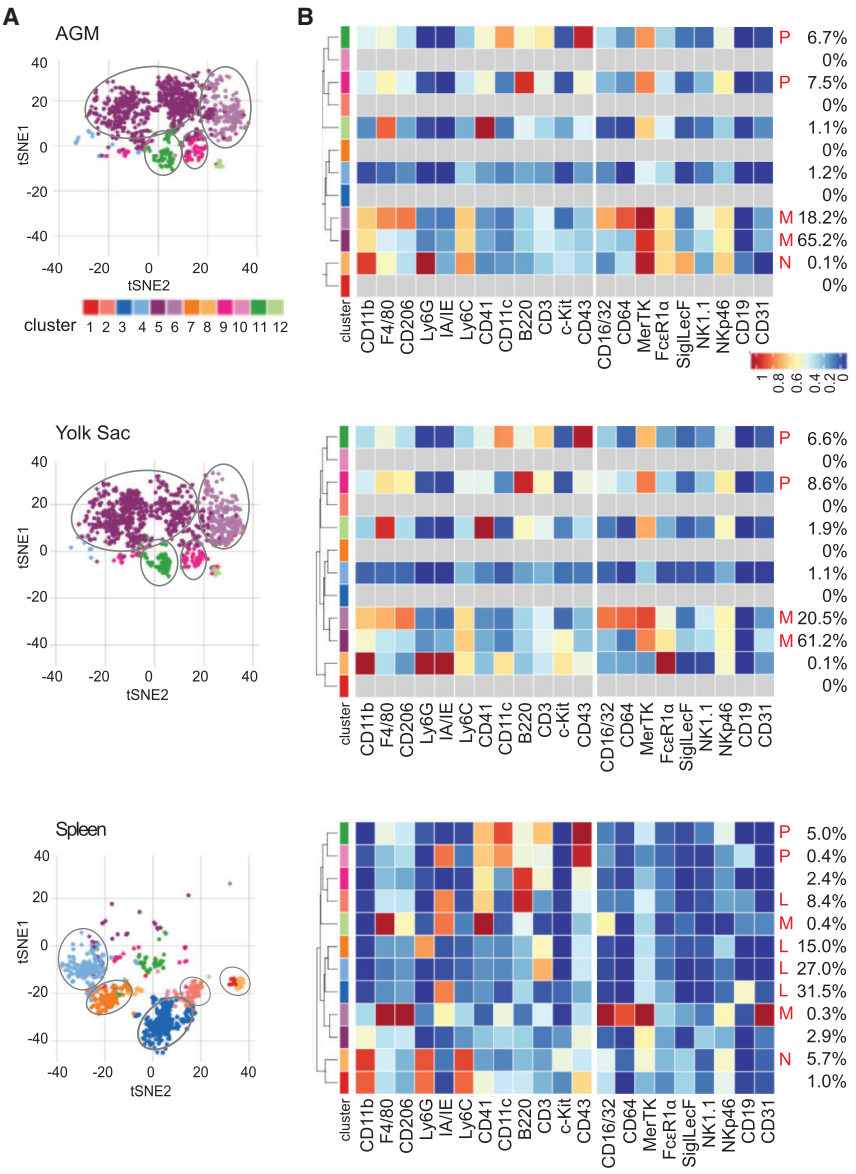

Figure 1. CyTOF Analysis of CD45$^+$ AGM, Yolk Sac, and Adult Spleen Cells

(A) tSNE clusters indicated by color (12 with >10 cells) of CD45$^+$ E10 AGM (top), E10 YS (middle) (n = 31, 31–37 sp) and adult spleen (bottom) cells based on 21 cell-surface markers.

(B) Heatmaps of surface-marker expression in CD45$^+$ AGM (top), YS (middle), and spleen (bottom) cells with percentages of cells in each tSNE cluster and lineage phenotype: N, neutrophils; M, macrophage and macrophage progenitor; L, lymphocytes and lymphoid progenitors, P, multipotential progenitor.

tissues, macrophages regulate steady-state hematopoiesis (Gordy et al., 2011), hematopoietic cell egress (Jaiswal et al., 2009), and erythrocyte maturation (Manwani and Bieker, 2008). They are best known for their innate immune pro- and anti-inflammatory functions in response to trauma, tissue damage, and tissue repair.

Some inflammatory molecules and cells have been implicated in the regulation of hematopoietic development in the embryo (Espín-Palazón et al., 2014; Li et al., 2014; North et al., 2007; Orelio et al., 2008). Interferon-γ (IFN-γ), interleukin-1β (IL-1β), tumor necrosis factor α (TNF-α), and matrix metalloproteases (Mmps) have been shown to enhance hematopoietic output in both zebrafish and mouse embryos, and neutrophils are the cellular effectors in zebrafish embryos. However, the identity of inflammatory cells in the mouse AGM microenvironment that may affect hematopoietic development is unclear. Macrophages are present in both mouse (Rae et al., 2007; Yokomizo et al., 2011) and E34-stage human embryos (Travnickova et al., 2015) along the aorta where HSCs emerge. Here, we examined the innate immune-cell composition of the mouse AGM HSC-generative microenvironment and show that macrophages were the most abundant hematopoietic cell type. We identified a CD206$^+$ pro-inflammatory macrophage subset that was highly dynamic and showed that macrophages were a crucial cellular component of the HSC inductive niche.

RESULTS

Macrophages Are the Most Abundant Hematopoietic Cells in the AGM

To investigate the cellular composition of the AGM microenvironment, we performed mass cytometry (CyTOF) on mouse E10.5 AGM cells. Cells were stained with metal-conjugated antibodies recognizing CD45 (pan-hematopoietic cell marker), hematopoietic lineage markers, and endothelial markers (Table S1; Key Resources Table). Adult mouse spleen served as control. Concatenated t-distributed stochastic neighbor embedding (tSNE) plots of AGM and spleen cells (Figure S1A) revealed different cluster distributions and frequencies. The AGM contained a few large unique CD45$^-$ cell clusters (10, 14, and 18), whereas most spleen cells were CD45$^+$ (Figure S1B). Flow cytometry analysis verified that only 0.47% ± 0.1% of AGM cells were CD45$^+$ (Figure S2). Hence, CyTOF analysis on unsorted AGM cells was not informative for hematopoietic cell composition.

To more-specifically characterize the AGM hematopoietic composition, CyTOF was performed on CD45$^+$ cells sorted from E10 AGM and YS tissues and an adult spleen. Concatenated tSNE plots (Figure 1A) revealed two major clusters of CD45$^+$ AGM cells in common with YS cells. Together, these two clusters represent 83.4% and 81.7% of the AGM and YS CD45$^+$ cells, respectively (Figure 1B). Two other smaller clusters of CD45$^+$ cells (14.2% in AGM and 15.2% in YS) were in common between these tissues. In contrast, spleen contained five major CD45$^+$ clusters (86.1% of cells) that were different from the clusters in the embryonic tissues

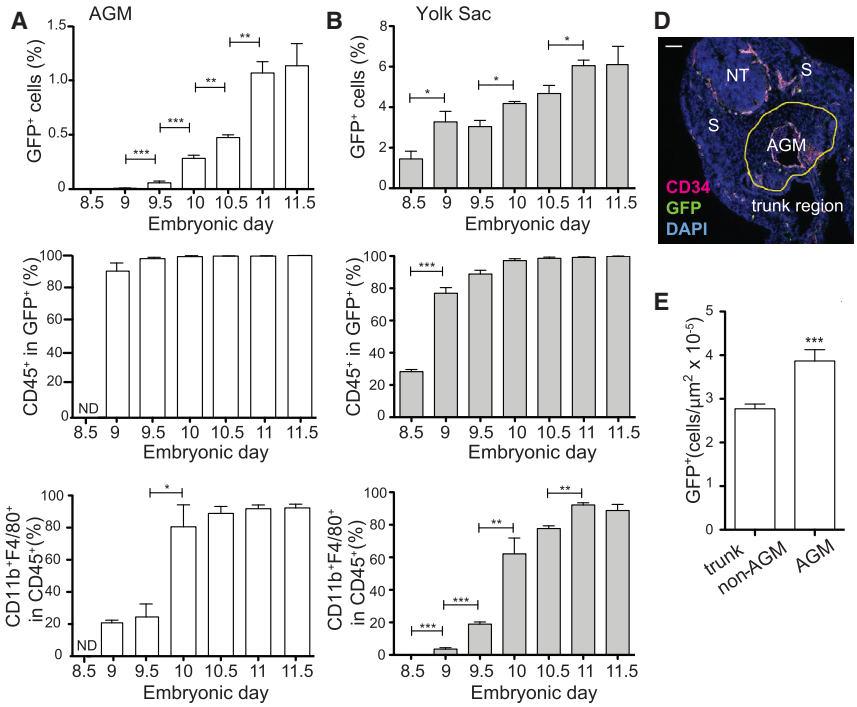

Figure 2. Appearance and Localization of AGM Myeloid Cells

(A and B) Flow cytometric analysis of E8.5 to E11.5 *MacGreen* (A) AGM and (B) YS cells. Percentage of GFP$^+$ cells (top), CD45$^+$ cells in GFP$^+$ fraction (middle), and CD11b$^+$F4/80$^+$ cells in CD45$^+$ fraction (bottom). Mean + SEM (n = 3/time, 2–4 AGM, 2–3 YS). ND, not done. One-way Anova with Bonferroni correction.

(C) Maximum projection confocal image of whole-mount E10 *MacGreen* embryo showing the trunk. A, aorta; V, vitelline artery. CD31$^+$ endothelium, gray; macrophages, green; c-Kit$^+$ IAHCs, magenta. Scale bar, 200 μm. High-magnification images of IAHC (right). Scale bars, 20 μm.

(D) Immunofluorescence of E10.5 *MacGreen* embryo transverse cryosection (10 μm) through aorta. AGM, aorta-gonad-mesonephros; NT, neural tube; S, somites. Yellow line, spatial boundaries of AGM. CD34$^+$ endothelium is in magenta, macrophages in green, and nuclei in blue (DAPI). Scale bar, 100 μm.

(E) Total number of macrophages per μm^2 in non-hematopoietic tissues of trunk (non-AGM) and AGM region. n = 40 (10 random sections, 4 embryos). The data are represented as mean + SEM. One-way Anova with Dunnett post-hoc test. *p < 0.05, **p < 0.01, ***p < 0.001. See Figures S3 and S4.

As shown in the heatmaps (Figure 1B), the major AGM and YS tSNE clusters corresponded to phenotypic macrophages or macrophage progenitors (M) expressing varying degrees of cluster of differentiation 11b (CD11b); F4/80; CD206; Ly6C; CD16/32; CD64; Mer proto-oncogenetyrosine kinase (MerTK); and Fc fragment of IgE receptor 1α (FcεR1α). The two smaller AGM and YS clusters appeared to be multilineage progenitors (P), as they expressed a combination of additional markers that included CD41, CD11c, B220, CD3, and CD43. Macrophages and macrophage progenitors were only 0.7% of the spleen CD45$^+$ population. Instead, both B and T lymphoid cells and lymphoid progenitors (L) made up four of the major populations, as defined by Ly6C, CD41, B220, CD3, and/or CD19 expression. The fifth major spleen CD45$^+$ population was composed of neutrophils (N), as defined by Ly6G expression. The AGM contained rare immature neutrophils (N). The AGM and YS contained no or undetectable mature lymphoid or other innate immune cells but had progenitor cells (overlapping with rare tSNE spleen clusters) that appeared to be lineage primed. E10 AGM and YS myeloid cells were separated into two major phenotypic macrophage clusters by CD206 expression: CD11b$^+$F4/80^{lo}CD206$^-$ cells were more frequent than CD11b$^+$F4/80$^+$CD206$^+$ cells. These macrophages and/or macrophage progenitors were the most abundant hematopoietic cell types in the embryonic tissues.

Macrophages Accumulate in the AGM Prior to HSC Production

The *MacGreen* (*Csf1rGFP*) transgenic mouse model facilitated vital imaging, localization, and isolation of AGM macrophages. Flow cytometry (CD45, CD11b, F4/80, Ly6C, Ly6G, CD3, B220, and MerTK; Figure S3A) revealed that all E10.5 AGM GFP$^+$ cells were CD45$^+$ and >95% of them were positive for CD11b, F4/80, and MerTK, common macrophage markers in the adult mouse. >99% of GFP$^+$ cells were negative for CD3 (T lymphocyte), B220 (B lymphocyte), and Ly6G (granulocyte) markers. Morphological examination (nucleus shape, cytoplasm) of Rapid Romanowsky stained cells confirmed that the majority of AGM GFP$^+$ cells were macrophages (Figure S3B). Out of 500 cells screened, 74% (371) were fully differentiated macrophages, 23% (115) were progenitors, and only 3% (15) were immature neutrophilic band cells (Figure S3C). Thus, the *MacGreen* reporter defines mainly macrophages in the embryo.

Macrophage appearance in *MacGreen* AGMs (E8.5 to E11.5) was assessed by flow cytometry (Figures 2A and S4A). No GFP$^+$ cells were found in the E8.5 AGM and very few were

detected at E9. The first AGM GFP$^+$ cells appeared at E9.5, and at E10 the percentage increased 5-fold ($p < 0.001$) just prior to the appearance of HSCs. GFP$^+$ cells continued to significantly increase from E10.5 (Figure 2A) and, thereafter, may have included some HSC (monocyte)-derived macrophages. Already at E9, most GFP$^+$ cells were CD45$^+$, but only 20% expressed the mature macrophage markers CD11b and F4/80. However, at E10, 80% of GFP$^+$ cells were positive for CD11b and F4/80 (Figure 2A). These results suggest that GFP$^+$ cells enter the AGM as progenitors and later become fully mature macrophages. This was supported by time-course analysis of the YS showing that 30% of GFP$^+$ cells present at E8.5 were CD45$^+$, but none expressed CD11b or F4/80 (Figures 2B and S4B). These were the predominant GFP$^+$ population in the YS until E9.5. Thereafter, the percentage of CD11b- and F4/80-expressing cells in the YS GFP$^+$CD45$^+$ fraction increased to 60%–95%. Together, these data suggest that AGM macrophages are derived from YS progenitors that enter and fully differentiate in the AGM.

GFP$^+$ macrophages were found in a punctate distribution within *MacGreen* E10.5 immunostained trunk regions (Figure 2C), consistent with CD45$^+$ and F4/80$^+$ cell distribution shown previously (Rae et al., 2007; Yokomizo et al., 2011). Macrophages were present throughout the trunk and AGM, and single GFP$^+$ macrophages were in close contact with aortic endothelial cells and intra-aortic hematopoietic cluster cells (IAHCs; CD31$^+$c-Kit$^+$) (Figure 2C, enlargements).

To quantitatively examine macrophage localization within the trunk region, E10.5 *MacGreen* transversal sections (10 μm) were immunostained for CD34 (Figure 2D). The number of GFP$^+$ cells/μm^2 was assessed in the AGM (with notochord, gut, and mesonephros as the dorsal, ventral, and lateral boundaries, respectively) and non-AGM trunk region. Significantly more macrophages were found in the AGM (near the IAHCs and aorta) than in the rest of the trunk region (Figure 2E; $p < 0.001$), consistent with findings in Zebrafish embryos (Travnickova et al., 2015).

Cx3cr1 Is Involved in Macrophage Progenitor Recruitment to the AGM

Chemokine receptors and chemokines are pivotal in mediating leukocyte recruitment to adult tissues (García-Ramallo et al., 2002; Mantovani et al., 2004). To identify what stimuli may attract macrophage progenitors to the AGM, we assessed the expression of chemokine receptors that are commonly found on adult macrophages (Ccr2, Ccr3, Ccr5, Ccr7, Cxcr2, Cxcr4, and Cx3cr1). Flow cytometric analysis of E10 and 10.5 *MacGreen* AGM (Figures 3A and S5A) and YS (Figures 3B and S5B) macrophages (GFP$^+$ cells) showed the highest expression of Cx3cr1. The other receptors were low or undetectable at E10. At E10.5, Ccr2 and Cxcr4 expression showed some increase on AGM and YS macrophages, and Ccr3 expression increased on YS macrophages.

Ligand expression was tested by semi-quantitative RT-PCR (*Ccl2*, *Ccl11*, *Ccl3*, *Cxcl12*, and *Cx3cl1*) on *MacGreen* AGM CD31$^+$GFP$^-$ cells (endothelial and IAHC) and GFP$^+$ macrophages (Figure 3C). Although *Ccl2*, *Ccl3*, and *Ccl11* transcripts were more abundant in AGM macrophages, *Cxcl12* and *Cx3cl1* were more highly expressed by CD31$^+$ AGM cells, suggesting that the elicitation of these chemokines by non-macrophage cell subsets acts to attract macrophages. To examine what CD31$^+$ AGM cells expressed *Cxcl12* and *Cx3cl1*, CD31$^+$ cells from *Ly6AGFP* AGMs (de Bruijn et al., 2002) were sorted according to GFP and c-Kit expression. This mouse transgenic reporter model allows high enrichment of endothelial (CD31$^+$GFP$^-$c-Kit$^-$), hematopoietic (CD31$^+$GFP$^-$c-kit$^+$), hematopoietic stem and/or progenitor (HS/PC) (CD31$^+$GFP$^+$c-Kit$^+$), and hemogenic endothelial cells (CD31$^+$GFP$^+$c-Kit$^-$) (Solaimani Kartalaei et al., 2015). Compared to endothelial cells, *Cxcl12* was 1.75-fold higher in hemogenic endothelial cells. Hematopoietic subpopulations (Figure 3D) showed lower expression. *Cx3cl1* expression was 2.5- to 3.2-fold higher in HS/PCs and hemogenic endothelial cells (Figure 3E) compared to the other cell fractions, suggesting a major involvement of Cx3cr1 in macrophage recruitment to nascent and emerging IAHCs.

To test this, we isolated AGM and YS cells from *Cx3cr1*$^{gfp/gfp}$ mice in which the insertion of the *GFP* gene results in a *Cx3cr1* null deletion (Jung et al., 2000). Flow cytometry analysis showed that the percentage of macrophages (CD45$^+$c-Kit$^-$CD11b$^+$F4/80$^+$) in *Cx3cr1*$^{gfp/gfp}$ AGMs was significantly lower than wild type and *Cx3cr1*$^{gfp/+}$ AGMs (Figure 3F, left). In contrast, the percentage of macrophages in the *Cx3cr1*$^{gfp/gfp}$ YS was significantly higher compared to those in wild-type YS (Figure 3F, right). The inverse correlation of macrophage percentages in the AGM versus YS suggested that the macrophage accumulation in the YS was due to a lack of Cx3cr1-related macrophage recruitment to the AGM.

The colony-forming unit (CFU)-C assay was performed on AGM cells from wild-type, *Cx3cr1*$^{gfp/+}$, and *Cx3cr1*$^{gfp/gfp}$ embryos to examine whether the percentage of macrophages in the AGM affected hematopoietic progenitor cell (HPC) numbers. A significant reduction in colony numbers (total, CFU-GEMM, and CFU-M) was found in *Cx3cr1*$^{gfp/gfp}$ AGMs compared to wild type, and there appeared to be a dosage effect on *Cx3cr1*$^{gfp/+}$ AGM colony output (Figure 3G). Thus, Cx3cr1-mediated macrophage recruitment to the AGM has a positive influence on AGM HPC output.

AGM-Associated Macrophages Dynamically Interact with Nascent and Emerging IAHCs

Since macrophages are motile cells, vital time-lapse microscopy (Boisset et al., 2010) was performed on thick embryo sections to examine macrophage dynamics within E10.5 *MacGreen* AGMs (Figure 4A). GFP$^+$ macrophages were found to be adjacent to and/or in direct contact with 28 out of 83 IAHCs (34%) examined (20 thick sections, $n = 4$). Within 75-min segment, macrophages were found to intravasate (through the aortic wall) to reach c-Kit$^+$ cells within the lumen (Figure 4B; Video S1). Macrophages were observed to interact for $\leq$3 h and push c-Kit$^+$ cells towards the aortic lumen (Figure 4C; Video S2). Moreover, some macrophages underwent cell division after "sensing" a portion of the aorta and, thereafter, each daughter macrophage moved and interacted with two separate CD31$^+$c-Kit$^+$ hematopoietic cells (Figure 4D; Video S3). These data show that highly motile AGM macrophages transiently interact with nascent and emerging IAHCs and suggest that such interactions directly influence HS/PC generation and/or maturation.

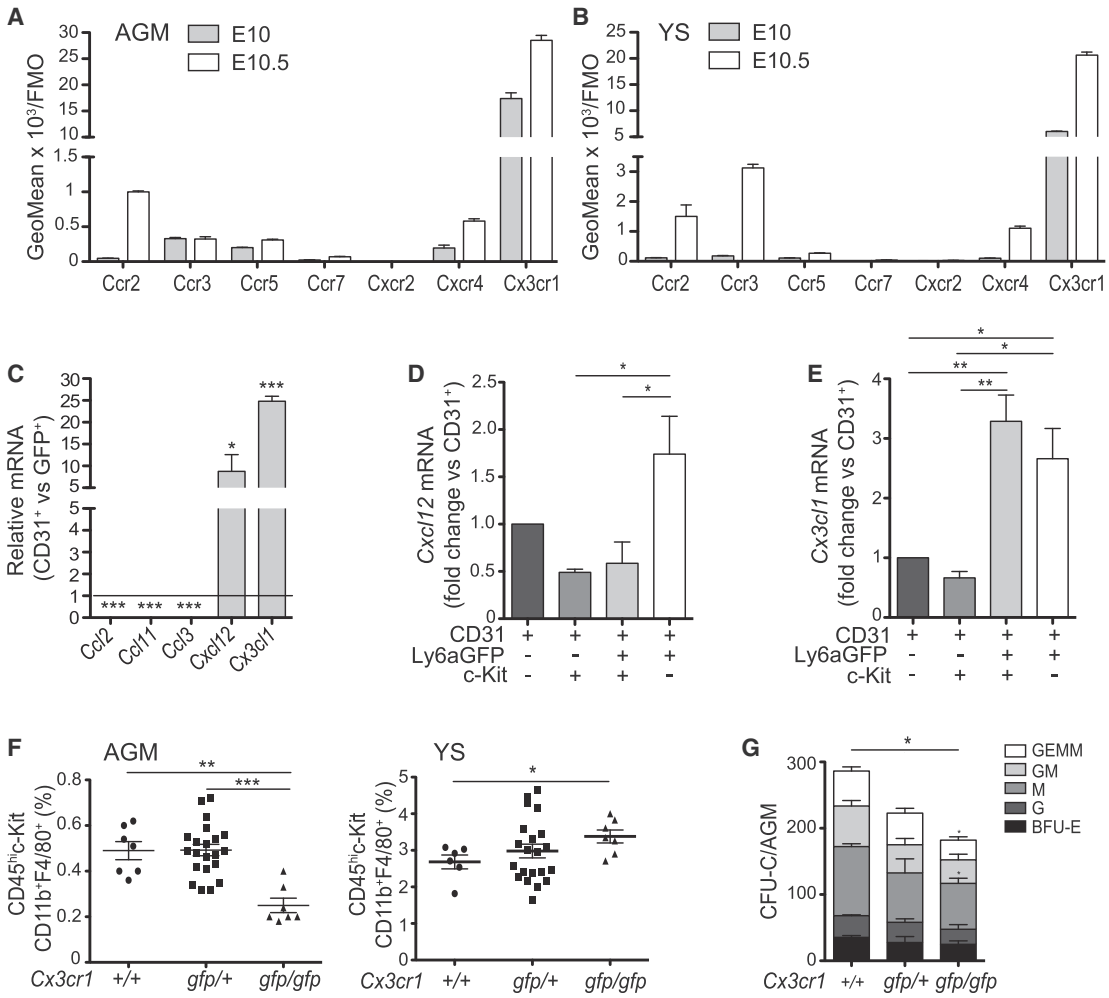

Figure 3. Macrophage Recruitment to the AGM is Cx3cr1 Mediated

(A and B) Cytofluorimetric analysis of chemokine receptors on (A) AGM and (B) YS macrophages of E10 and E10.5 *MacGreen* embryos. GeoMean over FMO (fluorescence minus one). Bars represent mean + SEM (n = 3, 2–3 AGM or YS/experiment).

(C) Semi-quantitative RT-PCR analysis of *Ccl2*, *Ccl11*, *Ccl3*, *Cxcl12*, and *Cx3cl1* in CD31$^+$ cells of E10.5 *MacGreen* AGM. Data are fold-change over the expression in GFP$^+$ cells, set as one (horizontal line). Bars represent mean + SEM (n = 3).

(D and E) Semi-quantitative RT-PCR analysis of (D) *Cxcl12* and (E) *Cx3cl1* in E10.5 *Ly6A-GFP* embryos. Data normalized to CD31$^+$ cells. Bars represent mean + SEM (n = 3).

(F) Cytofluorimetric percentages of macrophages (CD45$^+$c-Kit$^-$CD11b$^+$F4/80$^+$) in AGM (left) and YS (right) of E10.5 *Cx3cr1*$^{+/+}$ wild type, *Cx3cr1*$^{gfp/+}$, and *Cx3cr1*$^{gfp/gfp}$ embryos. Each symbol is an individual embryo. Error bars represent mean + SEM.

(G) CFU-C assay showing the number of colonies/AGM in E10.5 *Cx3cr1*$^{+/+}$, *Cx3cr1*$^{gfp/+}$, and *Cx3cr1*$^{gfp/gfp}$ embryos. BFU-E, burst forming unit-erythroid; CFU-G, CFU-granulocyte; CFU-M, CFU-macrophage; CFU-GM, CFU-granulocyte, macrophage; CFU-GEMM, CFU-granulocyte, erythrocyte, macrophage, megakaryocyte. Mean + SEM (n = 4).

(C and G) Student's t test; (D–F) one-way Anova with Bonferroni correction. *p < 0.05, **p < 0.01, ***p < 0.001. See Figure S5.

Hematopoietic Progenitor Cell Numbers Are Proportional to AGM Macrophage Percentages

The effect(s) of macrophages on AGM HPC output and function was examined using two macrophage depletion approaches (Figure 5A). In the first approach, BLZ945, an inhibitor of the colony stimulating factor 1 receptor (CSF1R) was added to E10.5 *MacGreen* AGM explant cultures. The overall viability of AGM explant cells after 72 h was unaffected by a range of BLZ945 concentrations (Figure 5B). However, a significant (55%–60%) decrease in macrophage percentages was observed in 6.7 μM and 67 μM BLZ945-treated AGM explants (Figure 5C), as compared to dimethyl sulfoxide (DMSO) control or 0.67 μM BLZ945-treated AGM explants. To test if macrophage depletion affected AGM HPC numbers, the CFU-C assay was performed. The total number of CFU-C and CFU-GEMM (granulocyte, erythrocyte, monocyte, megakaryocyte) per AGM was significantly decreased in 6.7-μM and 67-μM-treated explants compared to DMSO controls (Figure 5D), thus showing that AGM CFU-C numbers are directly related to the percentage of AGM macrophages.

In the second approach, apoptosis-inducing clodronate-liposomes (Pyonteck et al., 2013; Van Rooijen and Sanders, 1996) were used to achieve macrophage-specific depletion (Figure 5A).

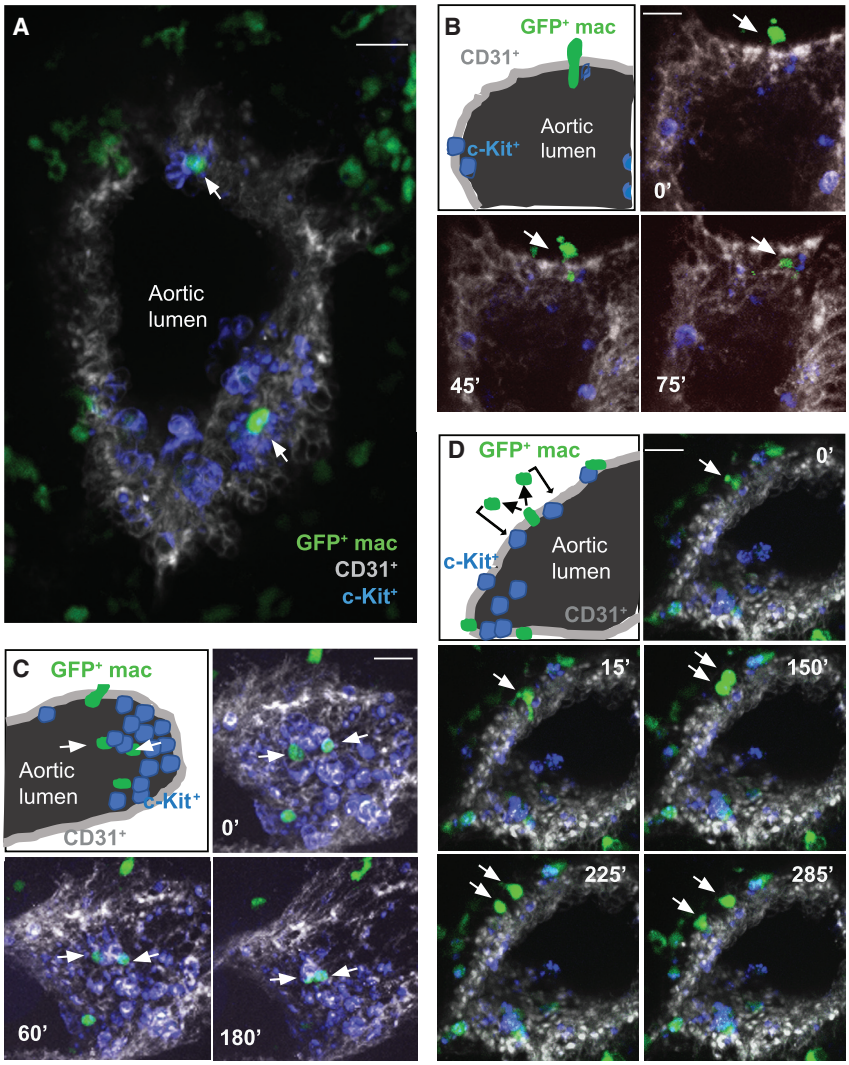

Figure 4. Macrophages Co-localize and Interact with IAHCs

(A and B) Immunofluorescence (A) and time-lapse imaging extracted time points (B) of transversal sections (150 μm) of E10.5 *MacGreen* embryos. Macrophages, green; $CD31^+$ endothelium, gray; c-Kit^+ cells, blue. Scale bars, 20 μm.

(B–D) Time is indicated at the top of each image. White arrows indicate the macrophages entering the aorta (B) or interacting with IAHCs (A, C, D). See Videos S1, S2, and S3.

AGM explants incubated 72 h with clodronate-liposomes showed no change in total AGM-cell viability compared to PBS-liposome-treated explants (Figure 5E), whereas macrophages ($CD45^+CD11b^+F4/80^+$) were decreased significantly by >70% (Figure 5F). Assessment of the HPC potential of the AGMs after clodronate-liposome treatment demonstrated a significant 43%–45% decrease in the total number of CFU-Cs, with a significant reduction in CFU-M and multipotent CFU-GEMM (Figure 5G) compared to control. To prove that the reduction of HPC potential was due to the absence of macrophages and not mediated by a direct effect of clodronate-liposomes on committed myeloid progenitors, the lymphoid potential of AGM HPC was assessed. AGM explants were incubated with clodronate or control PBS liposomes for 72 h, and the B lymphoid output was assessed after ten days of co-culture on OP9 cells (Figure S6A). No change in total AGM-cell viability was found (Figures S6B and S6C), and the percentage of macrophages ($CD45^+CD11b^+F4/80^+$) was decreased by 60% (Figures S6B and S6D) in clodronate-liposome-treated AGMs compared to the control. The percentages of $CD45^+B220^+$ (B cell progenitors) and $CD45^+B220^+CD19^+$ (mature B cells) populations were also decreased in the clodronate-liposome-treated co-cultures (Figures S6B, S6E, and S6F), demonstrating an effect of macrophage depletion on B lymphoid progenitors. The direct correlation between the percentage of macrophages and the number of HPCs, including multilineage and lymphoid progenitors in the AGM, supports a role for macrophages in promoting HPC generation.

AGM HSC Production Is Impaired in the Absence of Macrophages

BLZ945-inhibition and clodronate-liposome treatments were performed to test whether macrophages affect the production of AGM HSCs. Cells from BLZ945- or DMSO-treated AGM explants (Ly5.2 embryos; 37-39 sp) were intravenously injected into irradiated Ly5.1 adult mice. When donor-cell chimerism was assessed in the peripheral blood (PB) at 4 and 16 weeks post transplantation (Figure 5H), only 2 of 8 mice injected with BLZ945-treated AGM explant cells showed any PB donor-cell chimerism. In contrast, almost all (6 out of 8) recipients injected with control cells showed high percentages of donor-derived hematopoietic repopulation.

Similarly, cells from clodronate- and PBS-liposome-treated AGM explants (Ly5.2 embryos; 37-39 sp) were intravenously injected into irradiated Ly5.1 adult mice (Figure 5I). No donor-cell chimerism was found in the PB of 6 mice injected with clodronate-treated AGM explant cells at 4 and 16 weeks post-transplantation, whereas 4 out of 6 mice were reconstituted with cells from PBS-liposome-treated AGMs. Long-term multilineage engraftment was found in the bone marrow (BM), spleen, lymph node (LN), thymus, and PB of recipients of PBS control AGM cells, whereas no donor engraftment was found in recipients of clodronate-liposome-treated AGM cells (data not shown). Thus, macrophages play a role in the generation and/or maturation of HSCs in the mouse AGM.

CD206 Discriminates AGM-Associated Macrophages from Macrophage Progenitors

Further characterization of E10.5 AGM macrophages showed they were negative for Flk1 (Vegfr2; Yang et al., 2004), Tie2

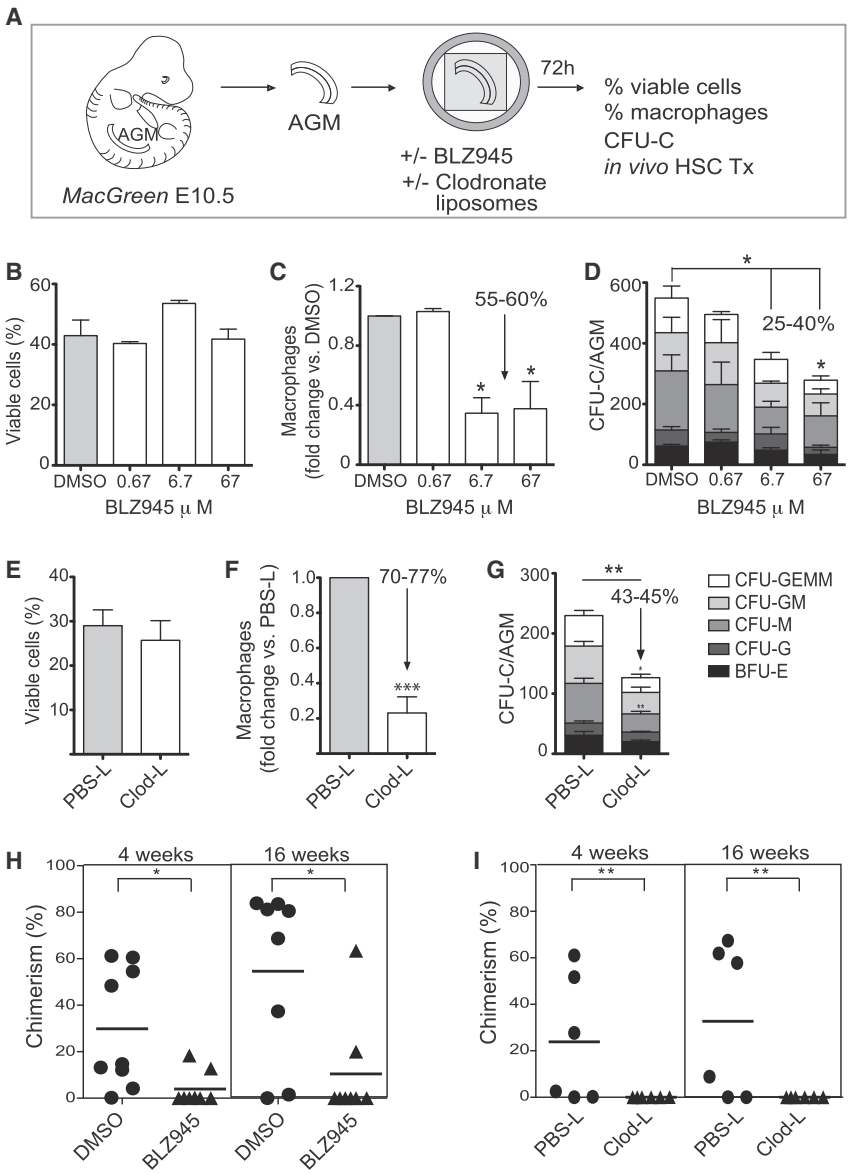

Figure 5. AGM HS/PC Are Reduced upon Macrophage Depletion

(A) Experimental set-up. CFU-C, colony forming unit in culture; Tx, transplantation. Cytofluorimetric percentages of (B and E) viable cells and (C and F) macrophages in AGM explants treated with BLZ945 (0.67, 6.7, or 67 μM) or clodronate-liposomes compared to controls. Arrow, reduction in macrophage percentages upon treatment. (D and G) CFU-C numbers per AGM explant upon BLZ945 or clodronate-liposome treatment compared to control with percentage reduction shown. BFU-E, burst forming unit-erythroid; CFU-G, colony forming unit-granulocyte; CFU-M, colony forming unit-macrophage; CFU-GM, colony forming unit-granulocyte, macrophage; CFU-GEMM, colony forming unit-granulocyte, erythrocyte, macrophage, megakaryocyte. PBS-L, PBS-liposomes; Clod-L, clodronate-liposomes. *In vivo* transplantation of (H) BLZ945-treated and (I) clodronate-liposome-treated AGM explant cells into irradiated adult Ly5.1 recipients. Chimerism (%CD45.2$^+$) in peripheral blood of recipients at 4 and 16 weeks post-transplant. Each symbol = one mouse. Triangles, BLZ945 or Clod-L treated AGMs; circles, controls (n = 3, Student's t test). (B, C, D, F, G) Mean + SEM (n = 4). (H, I) The horizontal lines represent the mean. *p < 0.05, **p < 0.01, ***p < 0.001. See Figure S6.

(angiopoietin receptor; Fukuhara et al., 2010), and IA/IE (histocompatibility molecule) (Figure 6A). However, ~50% of E10.5 AGM macrophages expressed CD206 (mannose receptor). CD206$^+$ macrophage percentages increased from E10 to E11 (Figure 6B). Cytospins of E10.5 *MacGreen* AGMs revealed that CD206$^+$ macrophages contain quantitatively more vacuoles than CD206$^-$ cells (Figure 6C), suggesting different maturation or activation states.

To test the states of GFP$^+$CD206$^+$ and GFP$^+$CD206$^-$ cells, chimeric co-cultures of OP9-DL1 stromal cells with cells sorted from *MacGreen* E10.5 AGMs were established and harvested after 1 week, and CD45$^+$ cells were examined for HPC activity (Figure 6D). Both CD206$^-$ and CD206$^+$ OP9-DL1 co-cultures yielded equivalent numbers of CD45$^+$ cells (not shown), and although the CD206$^-$ cell co-cultures produced all types of CFU-C, none were produced by the CD206$^+$ co-cultures (Figure 6D, left bars). Thus, CD206$^-$ cells are a mixed population of progenitors and macrophages, and the CD206$^+$ cells are fully mature macrophages (now defined as AGM-associated macrophages, AGM-aMs).

Spatial localization of AGM-aMs and CD206$^-$GFP$^+$ cells in E10.5 *MacGreen* AGM and non-AGM trunk regions was quantitatively assessed (Figure 6E). CD206$^-$GFP$^+$ cells were found in equal numbers/μm^2 in the non-AGM and AGM trunk regions and similar numbers of AGM-aMs/μm^2 were found in the non-AGM trunk region. However, the AGM contained significantly higher numbers of AGM-aMs/μm^2 (2.5-fold more). Moreover, some were engaged with aortic cells (Figure 6F), suggesting that AGM-aMs play a role in AGM HS/PC generation through interaction with nascent and emerging IAHCs.

AGM-Associated CD206$^+$ Macrophages Enhance Endothelial-to-Hematopoietic Transition

The influence of AGM-aMs and CD206$^-$GFP$^+$ cells on the hemogenic activity of E10.5 AGM endothelial cells (ECs, CD31^{+-}CD45$^-$CD41$^-$) was tested in chimeric co-cultures on OP9-DL1 cells (Figure 6D, right bars). Cell combinations included: ECs alone, ECs + CD206$^-$GFP$^+$, and ECs + AGM-aMs. After 1 week, cells were harvested and 5×10^3 CD45$^+$ cells were assayed for HPC activity. ECs alone yielded 203 ± 25 CFU-C. ECs + CD206$^-$GFP$^+$ cells yielded 311 ± 17 CFU-C (sum of EC-generated CFU-C [203 ± 25] plus CD206$^-$GFP$^+$-cell-generated CFU-C,106 ± 11) (Figure 6D, left bar). In contrast, ECs + AGM-aMs yielded 366 ± 13 CFU-C. As no CFU-Cs were generated by AGM-aMs in the absence of ECs (Figure 6D, left bar), the presence of AGM-aMs increased the CFU-C output of ECs by

56%. Moreover, a significant increase in CFU-M and CFU-GEMM was found in ECs + AGM-aMs compared to ECs alone (Figure 6D), indicating an inductive cooperation between AGM-aM and ECs in the generation of HPCs. To examine whether direct AGM-aM and EC interactions were required, we established transwell cultures. After 7 days, the same induced CFU-C output of ECs + AGM-aMs was observed in non-contact transwell conditions as seen in contact conditions (Figure 6G), suggesting that in prolonged cultures (as opposed to $\leq$3 h *in vivo* contact; Figure 4), the non-contact output is likely a result of soluble factor accumulation in the medium (see Discussion).

AGM-aMs Are Inflammatory and Transcriptionally Distinct from Macrophage Progenitors

RNA-sequencing datasets of *MacGreen* AGM GFP$^+$CD206$^+$ and GFP$^+$CD206$^-$ populations were compared. Unsupervised principal component analysis (PCA) (Figure 7A) showed AGM-aMs and GFP$^+$CD206$^-$ cells in two distinct clusters. Differentially expressed gene (DEG) analysis identified 1,265 genes (of 21,911) significantly altered with adjusted p value (false discovery rate, FDR) <0.05 in AGM-aMs compared to GFP$^+$CD206$^-$ cells (Table S2). Hierarchical clustering of the top 50 DEGs (Figure 7B) showed two distinct expression patterns (Table S3). Among 320 genes ($\log_2$FC1.5/$-$1.5, FDR $\leq$ 0.05), 147 were upregulated in AGM-aMs ($\log_2$FC $\geq$ 1.5, FDR $\leq$ 0.05) and showed a dominant inflammatory signature with a specific expression of *Ccl24*, *Ccl9*, *Igf1*, *Tnf*, *Bmp2*, *Pf4*, *Cxcl3*, *Gas6*, *Ccl12*, *Ccl7*, *Ccl2*, and *Il18* (Figure 7C). Validation of pro-inflammatory gene expression by qRT-PCR (Figure 7D) confirmed the upregulation of *Tnf*, *Ccl24*, *Ccl9*, *Igf1*, *Bmp2*, *Pf4*, *Ccl2*, and *Ccl7* in AGM-aMs and, thus, AGM-aMs contribute to the pro-inflammatory microenvironment of the AGM.

In addition, the relative expression of *Ifn*α, *Ifn*γ, and *Il1*β (previously reported to affect HS/PC generation in mouse and zebrafish embryos; Li et al., 2014) and *Mmp9* and *Mmp13* (metalloproteinases involved in extracellular matrix [ECM] degradation and aortic HS/PC mobilization in zebrafish embryos; Travnickova et al., 2015) was tested in AGM-aMs and GFP$^+$CD206$^-$ cells. No upregulated expression of the cytokines was found in AGM-aM compared to CD206$^-$ cells (Figure 7D), and a mixed "metalloproteinase signature" was found in both fractions (Figure 7E). However, *Mmp9* and *Mmp13* were significantly upregulated in AGM-aMs, as revealed by qRT-PCR (Figure 7F). Together, these data reveal that AGM-associated (CD206$^+$) macrophages play a positive role in the generation and/or maturation of HPCs and HSCs and may assist in ECM degradation.

DISCUSSION

We have shown that macrophages play a positive role in HSC generation. They are the most abundant innate immune cell type present in the AGM microenvironment prior to HSC generation and are pro-inflammatory. Macrophage progenitors generated in early waves of hematogenesis in the YS (Bertrand et al., 2005; Palis et al., 1999) are recruited through the Cx3cr1 signaling axis to the AGM, where they mature, express CD206, and dynamically interact with nascent and emerging aortic hematopoietic cells to influence AGM HS/PC production.

Phenotypic characterization of CD45$^+$ hematopoietic cell types in the AGM by CyTOF analysis for 21 hematopoietic lineage markers revealed little phenotypic heterogeneity. Of 7 clusters identified in tSNE and heatmap analyses, >83% of cells were phenotypic macrophages and macrophage progenitors. Whether these cells represent progenitors previously described, such as pre-macrophages (Stremmel et al., 2018) or EMPs (Frame et al., 2013; Palis et al., 1999) is uncertain. The CyTOF profiles of CD45$^+$ macrophage and progenitors (clusters 5 and 6) showed a high degree of similarity between the AGM and YS. The only detectable difference was the expression of c-Kit by YS CD11b$^+$F4/80$^-$CD206$^-$ cells (cluster 5), thus suggesting that heterogeneity or plasticity in macrophages in specific embryonic hematopoietic tissues is due to local microenvironment and/or differentiation state.

>14% of AGM CD45$^+$ cells (clusters 9 and 11) were phenotypic multipotent HPCs. These two clusters were found in the YS at a similar frequency and at a much lower frequency in the spleen with some marker variation. CD41 (embryonic progenitor and mature megakaryocytic marker) and CD43 (adult pan-leukocyte marker except resting B cells) were expressed by these cells in all three tissues. Cluster 9 cells co-expressing B220 and F4/80 were likely to be bi-potent macrophage B cell progenitors and functionally defined AGM myeloid-B lymphoid progenitors previously reported (Böiers et al., 2013; Godin et al., 1995; Katsura, 2002). Cluster 11 cells expressing CD11c, B220, CD3, and F4/80 were likely multipotent cells with innate immune fate for innate lymphoid cells (ILCs) and dendritic cells. Whether these embryonic cells are functionally similar to adult cells has yet to be established.

All major AGM and YS cell clusters (5, 6, 9, 11) highly expressed the MerTK macrophage marker, verifying that macrophages are the dominant AGM and YS hematopoietic cell type. In contrast, only rare spleen clusters (2, 5, 6) expressed MerTK. Low expression of NKp46 was also found in most of these clusters. In the adult, NKp46 is a marker for natural killer (NK) cells alongside NK1.1. However, no CD45$^+$ cells in the AGM, YS, or spleen were NK1.1$^+$. Because it is known that NK1.1$^+$ spleen cells are at low frequency and difficult to detect, it is as yet uncertain whether NK cells are present in embryonic tissues and/or whether the NKp46 marker is expressed by other non-NK-cell lineages. Similarly, no mature CD19$^+$ B cells were found in the AGM or YS. Although neutrophils and neutrophil progenitors make up about 10% of the spleen CD45$^+$ cell population (clusters 1 and 2), no cluster 1 and rare cluster 2 cells were found in the AGM and YS. Thus, the AGM and YS show a bias towards macrophages and progenitor cells, and CyTOF analysis with additional markers should aid in determining the heterogeneity within the embryonic progenitor populations.

As detected by fate mapping (Gomez Perdiguero et al., 2015), EMPs migrate from the YS to the caudal half of the mouse embryo between E8.5 and E9. We found that these early generated YS progenitors appear in the AGM by E9 already expressing the CD45 surface marker, but the CD11b and F4/80 mature macrophage markers were expressed only after arrival in the AGM. Macrophages accumulated in the AGM and were found to dynamically interact with nascent and emerging IAHCs. We confirmed that macrophage progenitor appearance in the AGM was, at least in part, Cx3cr1 mediated (Mass et al., 2016). However, since one-third of the total percentage of AGM macrophages is still detectable

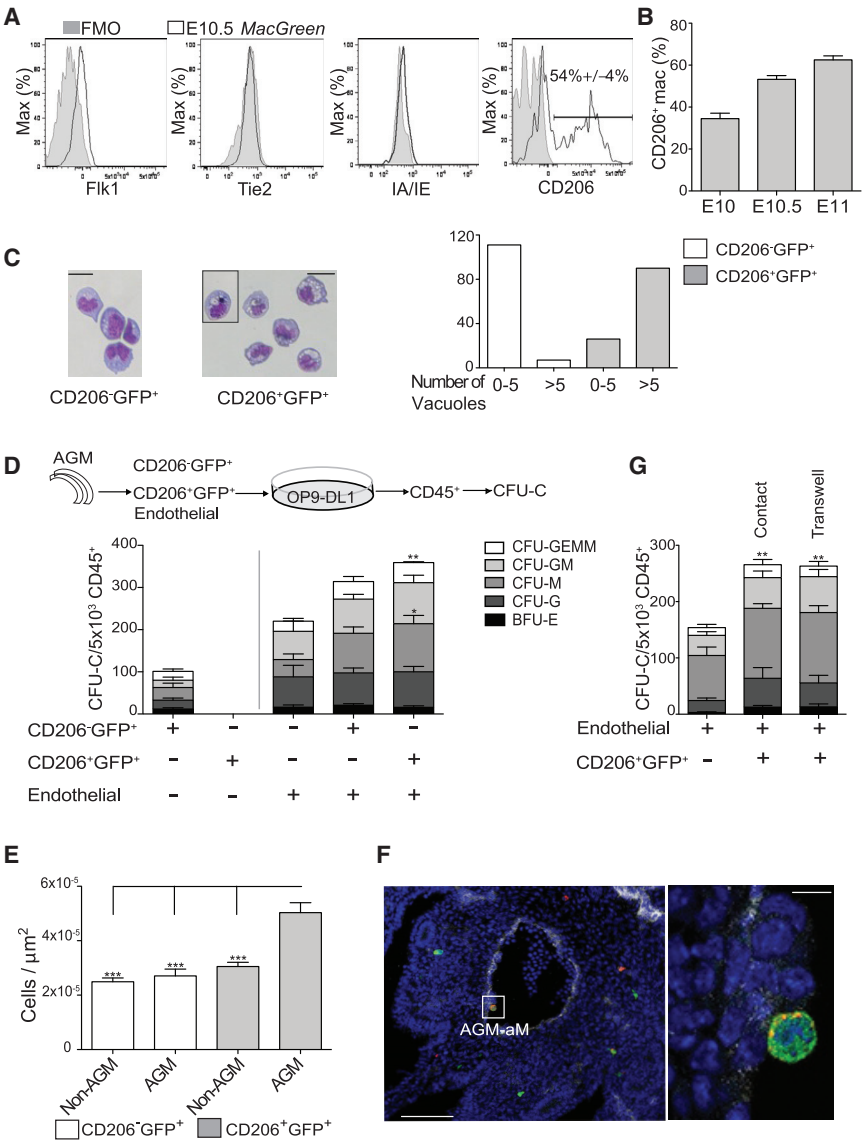

Figure 6. Majority of E10.5 AGM Macrophages are CD206$^+$

(A) Histograms (white), representative of 4 independent experiments, show percentages of AGM macrophages expressing Flk1, Tie2, IA/IE, and CD206 in E10.5 *MacGreen* embryos. FMO, gray.

(B) Time course of %CD206$^+$ cells in E10–E11 *MacGreen* AGM. The data are represented as mean + SEM (n = 3).

(C) Rapid Romanowsky staining of cytospun E10.5 *MacGreen* (CD45$^+$CD11b$^+$F4/80$^+$GFP$^+$CD206$^{+/-}$) macrophages. Left, GFP$^+$CD206$^-$; right, GFP$^+$ CD206$^+$ cells. Scale bar, 20 μm. Black box separates cells from different slides. Number of vacuoles in CD206$^-$GFP$^+$ cells (white bars) and CD206$^+$GFP$^+$ macrophages (gray bars). 100–120 cells/population scored.

(D) Schematic of OP9-DL1 co-culture experiments (top). CD206$^-$GFP$^+$=GFP$^+$CD45$^+$CD206$^-$; CD206$^+$GFP$^+$=GFP$^+$CD45$^+$CD206$^+$; EC, endothelial cells (CD45$^-$CD41$^-$CD31$^+$). Cell combinations plated on OP9-DL1 are indicated under the graph. Number of CFUs in culture (CFU-C) per 5×10^3 CD45$^+$ cells. BFU-E, burst forming unit-erythroid; CFU-G, colony forming unit-granulocyte; CFU-M, colony forming unit-macrophage; CFU-GM, colony forming unit-granulocyte, macrophage; CFU-GEMM, colony forming unit-granulocyte, erythrocyte, macrophage, megakaryocyte.

(E) Total number of CD206$^-$GFP$^+$ and CD206^{+-} GFP$^+$ cells/μm^2 in non-hematopoietic trunk region (non-AGM) and AGM. n = 40 (10 random sections, 4 embryos), two-way ANOVA with multiple comparisons corrected by a Tukey's range test, ***p < 0.001. The data are represented as mean + SEM.

(F) Fluorescent image of a representative E10.5 *MacGreen* transverse section (10 μm) showing an AGM-associated macrophage (AGM-aM) along the aortic wall (left). Scale bar, 100 μm. Boxed area is enlarged on the right; scale bar, 20 μm. CD34, white; CD206, red; GFP, green; and DAPI, blue.

(G) Number of CFU-C per 5×10^3 CD45$^+$ obtained after co-culturing CD206$^+$GFP$^+$ macrophages in contact with or separate from endothelial cells.

(D and G) mean + SEM (n = 4). Student's t test, *p < 0.05, **p < 0.01.

in *Cx3cr1*$^{-/-}$ mice, we suggest that other chemokines and chemokine receptors such as Cxcl12 and Cxcr4 may be involved.

Vital time-lapse imaging revealed the rapid interstitial movement of macrophages in and around the E10.5 aorta. We observed Csf1r$^+$ macrophages entering into the aortic lumen from the surrounding mesenchymal tissue of the AGM. This intravasation was in contrast with a recent report that YS macrophage progenitors colonize embryonic tissues through the circulation (extravasation) (Stremmel et al., 2018). Moreover, we showed that macrophages dynamically interacted with aortic CD31$^+$c-Kit$^+$ cluster cells. In some cases, a macrophage underwent cell division and the daughter cells interacted with adjacent or nearby aortic CD31$^+$c-Kit$^+$ cluster cells. The cell-cell interactions and possible regulatory cross-talk occurring transiently over a few short hours of developmental time (≤3 h) suggests a role(s) for macrophages in the process of HS/PC generation. The AGM HSC-generative microenvironment is present between E10 and E12, a time when the mouse embryo is undergoing rapid growth and remodeling (Yokomizo et al., 2011). Thus, we propose that direct contact of AGM-aMs with EC is needed *in vivo*, whereas AGM-aMs can regulate HS/PC generation in non-contact conditions *in vitro* through soluble signals to EC over many days.

The depletion of AGM macrophages with clodronate-liposomes and Csf1r inhibitor BLZ945 demonstrated that macrophages are indeed important for the production of HSCs. Others have reported that these treatments specifically deplete phagocytic cells *in vivo* (Pyonteck et al., 2013; Van Rooijen and Sanders, 1996). When AGM explants were treated *in vitro* for 3 days, both the clodronate-liposome and the BLZ945 treatment decreased the percentage of viable macrophages without affecting the overall viability of other AGM cells. The BLZ945 concentration normally used in cell cultures (0.67 μM) was insufficient to eliminate macrophages, likely due to the 3D mass of AGM explants. Depletion (~60%) was achieved with increased

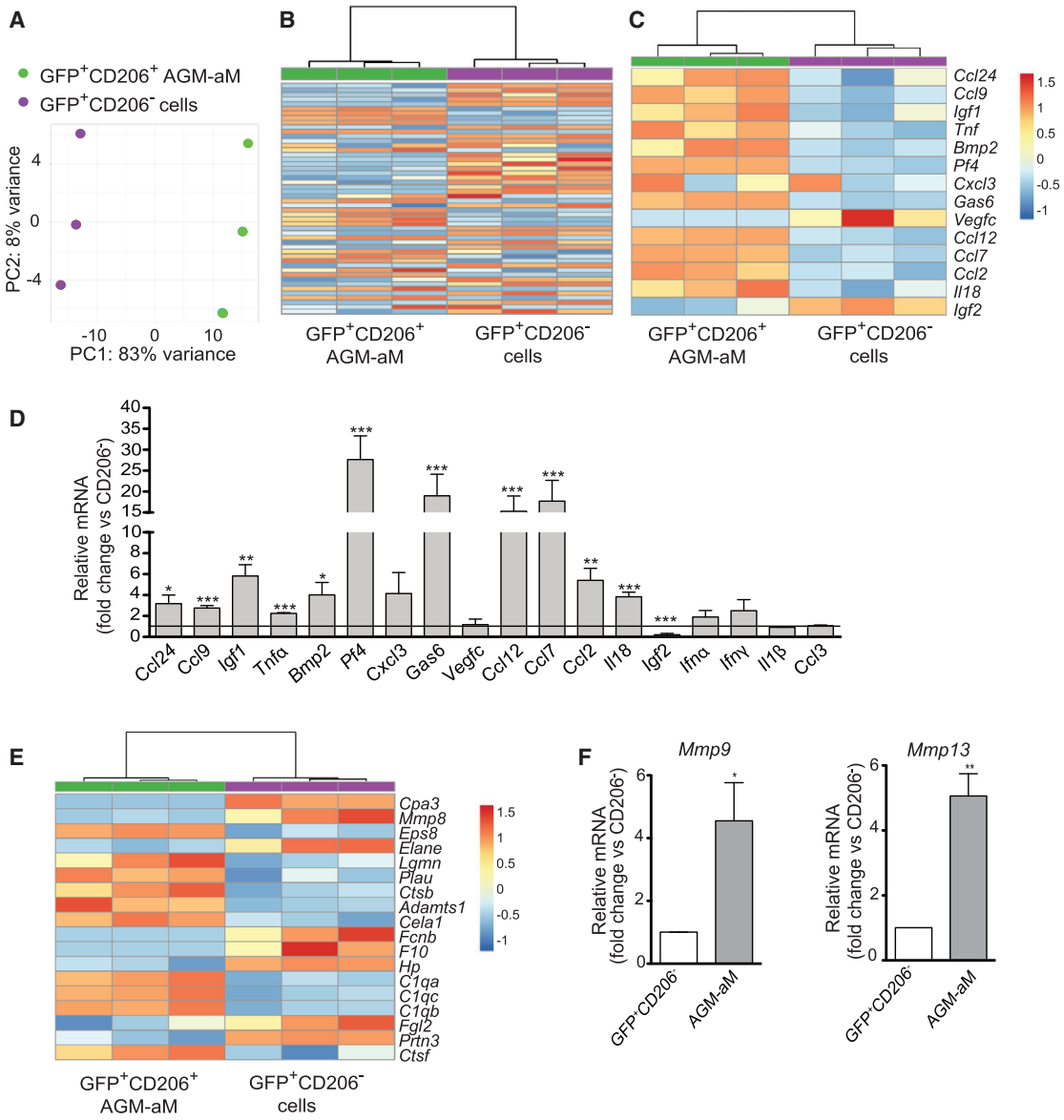

Figure 7. Transcriptomic Differences between CD206⁻ and CD206⁺ AGM Cells

(A) Principal component analysis (PCA) on all expressed genes in GFP⁺CD206⁺ (green) and GFP⁺CD206⁻ cells (purple) (n = 3, 4 AGMs/experiment).

(B–E) Heatmap calculated from the regularized log transformation counts of (B) the top 50 most variable genes, (C) cytokines, and (E) proteinases differentially expressed in GFP⁺CD206⁺ (green) and GFP⁺CD206⁻ (purple) AGM populations. Samples are clustered using average linkage and Pearson correlation. Samples are vertical and genes horizontal; red = upregulated and blue = downregulated genes. Semi-quantitative RT-PCR (mean + SEM) of (D) inflammatory factors (n = 5, 3–4 AGM/experiment) and (F) *Mmp9* (left) and *Mmp13* (right) (n = 5) in E10.5 *MacGreen* GFP⁺CD206⁻ and GFP⁺CD206⁺ cells. (D) Expression in CD206⁺ macrophages normalized over CD206⁻ cells (horizontal line).

(F) Expression in CD206⁺ macrophages (gray) normalized over CD206⁻ cells (white).

(D and F) Student's t test, *p < 0.05, **p < 0.01, ***p < 0.001. See Tables S2 and S3.

BLZ945 concentration but was still less effective than that mediated by clodronate liposomes (77%). These complementary methods revealed a direct correlation between the reduced macrophage percentages and the decreased number of multipotent HPC CFU-C and lymphoid progenitors compared to control explants. Importantly, the *in vivo* transplantation of clodronate-liposome- and BLZ945-treated AGM cells showed no or little donor-derived hematopoietic repopulation of adult irradiated mice. Despite reports that HSCs are Csf1r expressing, the fact that clodronate-liposome treatment eliminates macrophages and affects both HPC and HSC output of AGM explants strongly supports an active role for macrophages in the AGM HS/PC generative microenvironment.

Many groups over the years have attempted to develop macrophage-deficient mouse models. Pu.1-transcription-factor-deficient mice have no detectable embryonic macrophages, and depending on the deletion strategy, such mice die either by E18 (Scott et al., 1994) or within 48 h from birth (McKercher et al.,

1996). However, it is unknown whether *Pu.1*$^{-/-}$ AGM contains any YS-derived macrophages or AGM-aMs. Similarly, it is not known whether AGM-aMs are present in Csf1-deficient mice (*op/op*), which exhibit a general impairment in normal, steady-state hematopoiesis (Wiktor-Jedrzejczak et al., 1982). Only a small percentage (1%) of mature macrophages remain in *op/op* mice, and such mice appear to correct the hematopoietic defects as they age (Begg et al., 1993). With further characterization, these and newly developed models may be useful in establishing more complex chimeric cultures for studies of AGM HSC generation.

At least two types of myeloid populations exist in the AGM: macrophages expressing CD206 (mannose receptor) and CD206^{-} cells, which are a mixed population of macrophages and progenitors. CD206^{+} macrophages contain more vacuoles than the CD206^{-} cells and are more frequent in the AGM region compared to the rest of the embryo. The CD206 mannose receptor is a C-type lectin that functions in endocytosis and phagocytosis, playing an important role in immune homeostasis (Taylor et al., 2005). It is a marker of terminally differentiated macrophages in human (Mokoena and Gordon, 1985) and mouse embryonic macrophages by E10 (Takahashi et al., 1998). Mice deleted for the mannose receptor show major problems in the clearance of mannose-expressing proteins (Lee et al., 2002). The lack of fetal lethality in germline-deleted mice suggests that it does not affect the embryonic generation of the adult hematopoietic system and therefore serves only as a marker of AGM-aMs.

CD206 expression is generally accepted as an indicator of anti-inflammatory or "M2" macrophages in the adult mouse (Martinez et al., 2009; Rőszer, 2015). We found that AGM CD206^{+} macrophages expressed a pro-inflammatory signature. Of the pro-inflammatory molecules expressed by AGM-aMs, TNF-α is a modulator of HS/PC formation in zebrafish and mouse embryos (Espín-Palazón et al., 2014); Ccl24 (Ccr3 ligand) is upregulated in adult macrophages in TNF-α-rich environments and recruits eosinophils during asthma and allergic reactions (Lampinen et al., 2004); Ccl9 (macrophage inflammatory protein 1-γ or Ccr1 ligand) correlates with leukocyte recruitment in adult mice (Núñez et al., 2010); Igf1 (insulin-like growth factor 1) participates in immune-metabolic cross-talk in stress conditions (Spadaro et al., 2017) and promotes embryo and adult erythropoiesis (Kadri et al., 2015; Yumine et al., 2017); Bmp2 (bone morphogenic protein 2) is secreted by pro- and anti-inflammatory macrophages (Dube et al., 2017) and modulates human HSC proliferation *in vitro* (Bhatia et al., 1999); platelet factor 4 (Pf4, Cxcl4) attracts monocytes and neutrophils in inflammatory responses, supports hematopoietic cell survival, promotes macrophage maturation, and is expressed by HSCs in the mouse embryo (Calaminus et al., 2012); and Ccl2 and Ccl7 recruit leukocytes during inflammatory responses (Bardina et al., 2015). AGM-aMs did not express more IFN-γ and IL-1β (Espín-Palazón et al., 2014; Kim et al., 2016; Li et al., 2014; Orelio et al., 2008; Z.L., unpublished data) than CD206^{-}cells suggesting that these cytokines may be produced by either cell subset. It will be noteworthy to examine what specific roles these pro-inflammatory molecules play *in vivo* in the AGM, alone and in combination with each other and factors produced by other microenvironmental cells.

It is important to note that our results on pro-inflammatory AGM-aMs are in contrast with those in zebrafish embryos, where proinflammatory cytokines are produced mainly by neutrophils (Espín-Palazón et al., 2014). Rare immature neutrophilic band cells were found in our cytospins and are likely to be the minor Ly6G^{+} population seen by CyTOF. These immature cells are not phagocytic. Thus, they would not be eliminated during clodronate-liposome treatment that hence should have resulted in an increase in HSC and HPC numbers, not a decrease. We cannot completely rule out the influence of immature neutrophil band cells on HPCs because, after clodronate-liposome treatment, some HPCs (but no HSCs) were still present in the cultures. In Zebrafish embryos, macrophages have been found to dynamically interact with aortic hematopoietic cells and produce Mmp9 and Mmp13, which degrade the ECM to mobilize the emerging cells (Travnickova et al., 2015). We too have found expression of these Mmps in mouse AGM-aMs and suggest that these pro-inflammatory macrophages play an additional role to mobilize the aortic hematopoietic clusters of the mouse embryo.

Taken together, our data in the mouse embryo show that AGM-associated macrophages expressing the mannose receptor and pro-inflammatory molecules dynamically interact with nascent and emerging aortic cluster cells to affect HPC and HSC production in the AGM. These AGM-associated macrophages elaborate signals that likely affect processes such as HS/PC fate decisions, HS/PC function, ECM degradation, and/or mobilization of newly generated HS/PC. Our results provide a starting point for approaches with these macrophages to recreate the dynamic *in vivo* developmental microenvironment for the *de novo* production of robust HSCs.

STAR★METHODS

Detailed methods are provided in the online version of this paper and include the following:

- KEY RESOURCES TABLE
- CONTACT FOR REAGENT AND RESOURCE SHARING
- EXPERIMENTAL MODEL AND SUBJECT DETAILS
- METHOD DETAILS
  - Mouse and embryo generation
  - Mass cytometry (CyTOF)
  - Mass cytometry statistical analysis
  - Whole-mount Images
  - Tissue Sections
  - Time-lapse *ex vivo* imaging
  - AGM explant cultures
  - CFU-C assay and stem cell transplantation
  - OP9/OP9-DL1 co-culture system
  - BLZ945 and Clodronate-liposome treatment
  - Flow analysis and sorting
  - Gene Expression Analysis
  - RNA-seq
  - Sequencing alignment and Quantification
  - Statistical analysis for differentially expressed genes
- QUANTIFICATION AND STATISTICAL ANALYSIS
- DATA AND SOFTWARE AVAILABILITY

SUPPLEMENTAL INFORMATION

Supplemental Information can be found online at https://doi.org/10.1016/j.immuni.2019.05.003.

ACKNOWLEDGMENTS

We thank lab members for critical comments, C. Rodriguez-Seoane for technical assistance; C. Eich for vital imaging support; M.T. Fontán-Yanes for helping with the time-course experiment; the QMRI flow cytometry and cell sorting facility (S. Johnston, W. Ramsay, and M. Pattison); and T. Gillespie and D. Soong for microscopy expertise. Support provided by ERC AdG 341096 to E.D.

AUTHOR CONTRIBUTIONS

S.A.M. performed the research; Z.L. helped with the transplantation and the co-culture experiments; S.R. performed the immunofluorescence experiments; C.K. and M.R. ran and analyzed the CyTOF data; S.F. analyzed the RNA-seq; C.S.V. provided technical help; J.W.P. provided mice; S.A.M. and E.D. designed the study, interpreted data, and wrote the manuscript.

DECLARATION OF INTERESTS

The authors declare no competing interests.

Received: June 28, 2018
Revised: March 4, 2019
Accepted: May 11, 2019
Published: June 6, 2019

REFERENCES

Bardina, S.V., Michlmayr, D., Hoffman, K.W., Obara, C.J., Sum, J., Charo, I.F., Lu, W., Pletnev, A.G., and Lim, J.K. (2015). Differential Roles of Chemokines CCL2 and CCL7 in Monocytosis and Leukocyte Migration during West Nile Virus Infection. J. Immunol. *195*, 4306–4318.

Begg, S.K., Radley, J.M., Pollard, J.W., Chisholm, O.T., Stanley, E.R., and Bertoncello, I. (1993). Delayed hematopoietic development in osteopetrotic (op/op) mice. J. Exp. Med. *177*, 237–242.

Bertrand, J.Y., Jalil, A., Klaine, M., Jung, S., Cumano, A., and Godin, I. (2005). Three pathways to mature macrophages in the early mouse yolk sac. Blood *106*, 3004–3011.

Bhatia, M., Bonnet, D., Wu, D., Murdoch, B., Wrana, J., Gallacher, L., and Dick, J.E. (1999). Bone morphogenetic proteins regulate the developmental program of human hematopoietic stem cells. J. Exp. Med. *189*, 1139–1148.

Böiers, C., Carrelha, J., Lutteropp, M., Luc, S., Green, J.C., Azzoni, E., Woll, P.S., Mead, A.J., Hultquist, A., Swiers, G., et al. (2013). Lymphomyeloid contribution of an immune-restricted progenitor emerging prior to definitive hematopoietic stem cells. Cell Stem Cell *13*, 535–548.

Boisset, J.C., van Cappellen, W., Andrieu-Soler, C., Galjart, N., Dzierzak, E., and Robin, C. (2010). In vivo imaging of haematopoietic cells emerging from the mouse aortic endothelium. Nature *464*, 116–120.

Calaminus, S.D., Guitart, A.V., Sinclair, A., Schachtner, H., Watson, S.P., Holyoake, T.L., Kranc, K.R., and Machesky, L.M. (2012). Lineage tracing of Pf4-Cre marks hematopoietic stem cells and their progeny. PLoS ONE *7*, e51361.

Charbord, P., Pouget, C., Binder, H., Dumont, F., Stik, G., Levy, P., Allain, F., Marchal, C., Richter, J., Uzan, B., et al. (2014). A systems biology approach for defining the molecular framework of the hematopoietic stem cell niche. Cell Stem Cell *15*, 376–391.

Chen, M.J., Li, Y., De Obaldia, M.E., Yang, Q., Yzaguirre, A.D., Yamada-Inagawa, T., Vink, C.S., Bhandoola, A., Dzierzak, E., and Speck, N.A. (2011). Erythroid/myeloid progenitors and hematopoietic stem cells originate from distinct populations of endothelial cells. Cell Stem Cell *9*, 541–552.

Crisan, M., Kartalaei, P.S., Vink, C.S., Yamada-Inagawa, T., Bollerot, K., van IJcken, W., van der Linden, R., de Sousa Lopes, S.M., Monteiro, R., Mummery, C., and Dzierzak, E. (2015). BMP signalling differentially regulates distinct haematopoietic stem cell types. Nat. Commun. *6*, 8040.

de Bruijn, M.F., Speck, N.A., Peeters, M.C., and Dzierzak, E. (2000). Definitive hematopoietic stem cells first develop within the major arterial regions of the mouse embryo. EMBO J. *19*, 2465–2474.

de Bruijn, M.F., Ma, X., Robin, C., Ottersbach, K., Sanchez, M.J., and Dzierzak, E. (2002). Hematopoietic stem cells localize to the endothelial cell layer in the midgestation mouse aorta. Immunity *16*, 673–683.

Dobin, A., Davis, C.A., Schlesinger, F., Drenkow, J., Zaleski, C., Jha, S., Batut, P., Chaisson, M., and Gingeras, T.R. (2013). STAR: ultrafast universal RNA-seq aligner. Bioinformatics *29*, 15–21.

Doulatov, S., Vo, L.T., Chou, S.S., Kim, P.G., Arora, N., Li, H., Hadland, B.K., Bernstein, I.D., Collins, J.J., Zon, L.I., and Daley, G.Q. (2013). Induction of multipotential hematopoietic progenitors from human pluripotent stem cells via respecification of lineage-restricted precursors. Cell Stem Cell *13*, 459–470.

Dube, P.R., Birnbaumer, L., and Vazquez, G. (2017). Evidence for constitutive bone morphogenetic protein-2 secretion by M1 macrophages: Constitutive auto/paracrine osteogenic signaling by BMP-2 in M1 macrophages. Biochem. Biophys. Res. Commun. *491*, 154–158.

Durand, C., Robin, C., Bollerot, K., Baron, M.H., Ottersbach, K., and Dzierzak, E. (2007). Embryonic stromal clones reveal developmental regulators of definitive hematopoietic stem cells. Proc. Natl. Acad. Sci. USA *104*, 20838–20843.

Dzierzak, E., and Bigas, A. (2018). Blood Development: Hematopoietic Stem Cell Dependence and Independence. Cell Stem Cell *22*, 639–651.

Espín-Palazón, R., Stachura, D.L., Campbell, C.A., García-Moreno, D., Del Cid, N., Kim, A.D., Candel, S., Meseguer, J., Mulero, V., and Traver, D. (2014). Proinflammatory signaling regulates hematopoietic stem cell emergence. Cell *159*, 1070–1085.

Finck, R., Simonds, E.F., Jager, A., Krishnaswamy, S., Sachs, K., Fantl, W., Pe'er, D., Nolan, G.P., and Bendall, S.C. (2013). Normalization of mass cytometry data with bead standards. Cytometry A *83*, 483–494.

Fitch, S.R., Kimber, G.M., Wilson, N.K., Parker, A., Mirshekar-Syahkal, B., Göttgens, B., Medvinsky, A., Dzierzak, E., and Ottersbach, K. (2012). Signaling from the sympathetic nervous system regulates hematopoietic stem cell emergence during embryogenesis. Cell Stem Cell *11*, 554–566.

Frame, J.M., McGrath, K.E., and Palis, J. (2013). Erythro-myeloid progenitors: "definitive" hematopoiesis in the conceptus prior to the emergence of hematopoietic stem cells. Blood Cells Mol. Dis. *51*, 220–225.

Fukuhara, S., Sako, K., Noda, K., Zhang, J., Minami, M., and Mochizuki, N. (2010). Angiopoietin-1/Tie2 receptor signaling in vascular quiescence and angiogenesis. Histol. Histopathol. *25*, 387–396.

García-Ramallo, E., Marques, T., Prats, N., Beleta, J., Kunkel, S.L., and Godessart, N. (2002). Resident cell chemokine expression serves as the major mechanism for leukocyte recruitment during local inflammation. J. Immunol. *169*, 6467–6473.

Godin, I., Dieterlen-Lièvre, F., and Cumano, A. (1995). B-lymphoid potential in pre-liver mouse embryo. Semin. Immunol. *7*, 131–141.

Gomez Perdiguero, E., Klapproth, K., Schulz, C., Busch, K., Azzoni, E., Crozet, L., Garner, H., Trouillet, C., de Bruijn, M.F., Geissmann, F., and Rodewald, H.R. (2015). Tissue-resident macrophages originate from yolk-sac-derived erythro-myeloid progenitors. Nature *518*, 547–551.

Gordy, C., Pua, H., Sempowski, G.D., and He, Y.W. (2011). Regulation of steady-state neutrophil homeostasis by macrophages. Blood *117*, 618–629.

Hume, D.A., Perry, V.H., and Gordon, S. (1983). Immunohistochemical localization of a macrophage-specific antigen in developing mouse retina: phagocytosis of dying neurons and differentiation of microglial cells to form a regular array in the plexiform layers. J. Cell Biol. *97*, 253–257.

Jaffredo, T., Gautier, R., Eichmann, A., and Dieterlen-Lièvre, F. (1998). Intraaortic hemopoietic cells are derived from endothelial cells during ontogeny. Development *125*, 4575–4583.

Jaiswal, S., Jamieson, C.H., Pang, W.W., Park, C.Y., Chao, M.P., Majeti, R., Traver, D., van Rooijen, N., and Weissman, I.L. (2009). CD47 is upregulated on circulating hematopoietic stem cells and leukemia cells to avoid phagocytosis. Cell *138*, 271–285.

Jung, S., Aliberti, J., Graemmel, P., Sunshine, M.J., Kreutzberg, G.W., Sher, A., and Littman, D.R. (2000). Analysis of fractalkine receptor CX(3)CR1 function by targeted deletion and green fluorescent protein reporter gene insertion. Mol. Cell. Biol. *20*, 4106–4114.

Kadri, Z., Lefevre, C., Goupille, O., Penglong, T., Granger-Locatelli, M., Fucharoen, S., Maouche-Chretien, L., Leboulch, P., and Chretien, S. (2015). Erythropoietin and IGF-1 signaling synchronize cell proliferation and maturation during erythropoiesis. Genes Dev. *29*, 2603–2616.

Katsura, Y. (2002). Redefinition of lymphoid progenitors. Nat. Rev. Immunol. *2*, 127–132.

Kim, P.G., Canver, M.C., Rhee, C., Ross, S.J., Harriss, J.V., Tu, H.C., Orkin, S.H., Tucker, H.O., and Daley, G.Q. (2016). Interferon-α signaling promotes embryonic HSC maturation. Blood *128*, 204–216.

Krieg, C., Nowicka, M., Guglietta, S., Schindler, S., Hartmann, F.J., Weber, L.M., Dummer, R., Robinson, M.D., Levesque, M.P., and Becher, B. (2018). High-dimensional single-cell analysis predicts response to anti-PD-1 immunotherapy. Nat. Med. *24*, 144–153.

Lampinen, M., Carlson, M., Håkansson, L.D., and Venge, P. (2004). Cytokine-regulated accumulation of eosinophils in inflammatory disease. Allergy *59*, 793–805.

Lee, S.J., Evers, S., Roeder, D., Parlow, A.F., Risteli, J., Risteli, L., Lee, Y.C., Feizi, T., Langen, H., and Nussenzweig, M.C. (2002). Mannose receptor-mediated regulation of serum glycoprotein homeostasis. Science *295*, 1898–1901.

Leid, J., Carrelha, J., Boukarabila, H., Epelman, S., Jacobsen, S.E., and Lavine, K.J. (2016). Primitive Embryonic Macrophages are Required for Coronary Development and Maturation. Circ. Res. *118*, 1498–1511.

Li, Y., Esain, V., Teng, L., Xu, J., Kwan, W., Frost, I.M., Yzaguirre, A.D., Cai, X., Cortes, M., Maijenburg, M.W., et al. (2014). Inflammatory signaling regulates embryonic hematopoietic stem and progenitor cell production. Genes Dev. *28*, 2597–2612.

Liao, Y., Smyth, G.K., and Shi, W. (2014). featureCounts: an efficient general purpose program for assigning sequence reads to genomic features. Bioinformatics *30*, 923–930.

Mantovani, A., Sica, A., Sozzani, S., Allavena, P., Vecchi, A., and Locati, M. (2004). The chemokine system in diverse forms of macrophage activation and polarization. Trends Immunol. *25*, 677–686.

Manwani, D., and Bieker, J.J. (2008). The erythroblastic island. Curr. Top. Dev. Biol. *82*, 23–53.

Martinez, F.O., Helming, L., and Gordon, S. (2009). Alternative activation of macrophages: an immunologic functional perspective. Annu. Rev. Immunol. *27*, 451–483.

Mass, E., Ballesteros, I., Farlik, M., Halbritter, F., Günther, P., Crozet, L., Jacome-Galarza, C.E., Händler, K., Klughammer, J., Kobayashi, Y., et al. (2016). Specification of tissue-resident macrophages during organogenesis. Science *353*, aaf4238.

McKercher, S.R., Torbett, B.E., Anderson, K.L., Henkel, G.W., Vestal, D.J., Baribault, H., Klemsz, M., Feeney, A.J., Wu, G.E., Paige, C.J., and Maki, R.A. (1996). Targeted disruption of the PU.1 gene results in multiple hematopoietic abnormalities. EMBO J. *15*, 5647–5658.

Medvinsky, A., and Dzierzak, E. (1996). Definitive hematopoiesis is autonomously initiated by the AGM region. Cell *86*, 897–906.

Mei, H.E., Leipold, M.D., Schulz, A.R., Chester, C., and Maecker, H.T. (2015). Barcoding of live human peripheral blood mononuclear cells for multiplexed mass cytometry. J. Immunol. *194*, 2022–2031.

Mokoena, T., and Gordon, S. (1985). Human macrophage activation. Modulation of mannosyl, fucosyl receptor activity in vitro by lymphokines, gamma and alpha interferons, and dexamethasone. J. Clin. Invest. *75*, 624–631.

Munro, D.A.D., Wineberg, Y., Tarnick, J., Vink, C.S., Li, Z., Pridans, C., Dzierzak, E., Kalisky, T., Hohenstein, P., and Davies, J.A. (2019). Macrophages restrict the nephrogenic field and promote endothelial connections during kidney development. eLife *8*, e43271.

North, T.E., Goessling, W., Walkley, C.R., Lengerke, C., Kopani, K.R., Lord, A.M., Weber, G.J., Bowman, T.V., Jang, I.H., Grosser, T., et al. (2007). Prostaglandin E2 regulates vertebrate haematopoietic stem cell homeostasis. Nature *447*, 1007–1011.

Nowicka, M., Krieg, C., Weber, L.M., Hartmann, F.J., Guglietta, S., Becher, B., Levesque, M.P., and Robinson, M.D. (2017). CyTOF workflow: differential discovery in high-throughput high-dimensional cytometry datasets. F1000Res. *6*, 748.

Núñez, V., Alameda, D., Rico, D., Mota, R., Gonzalo, P., Cedenilla, M., Fischer, T., Boscá, L., Glass, C.K., Arroyo, A.G., and Ricote, M. (2010). Retinoid X receptor alpha controls innate inflammatory responses through the up-regulation of chemokine expression. Proc. Natl. Acad. Sci. USA *107*, 10626–10631.

Orelio, C., Haak, E., Peeters, M., and Dzierzak, E. (2008). Interleukin-1-mediated hematopoietic cell regulation in the aorta-gonad-mesonephros region of the mouse embryo. Blood *112*, 4895–4904.

Palis, J., Robertson, S., Kennedy, M., Wall, C., and Keller, G. (1999). Development of erythroid and myeloid progenitors in the yolk sac and embryo proper of the mouse. Development *126*, 5073–5084.

Peeters, M., Ottersbach, K., Bollerot, K., Orelio, C., de Bruijn, M., Wijgerde, M., and Dzierzak, E. (2009). Ventral embryonic tissues and Hedgehog proteins induce early AGM hematopoietic stem cell development. Development *136*, 2613–2621.

Picelli, S., Björklund, A.K., Faridani, O.R., Sagasser, S., Winberg, G., and Sandberg, R. (2013). Smart-seq2 for sensitive full-length transcriptome profiling in single cells. Nat. Methods *10*, 1096–1098.

Pyonteck, S.M., Akkari, L., Schuhmacher, A.J., Bowman, R.L., Sevenich, L., Quail, D.F., Olson, O.C., Quick, M.L., Huse, J.T., Teijeiro, V., et al. (2013). CSF-1R inhibition alters macrophage polarization and blocks glioma progression. Nat. Med. *19*, 1264–1272.

Rae, F., Woods, K., Sasmono, T., Campanale, N., Taylor, D., Ovchinnikov, D.A., Grimmond, S.M., Hume, D.A., Ricardo, S.D., and Little, M.H. (2007). Characterisation and trophic functions of murine embryonic macrophages based upon the use of a Csf1r-EGFP transgene reporter. Dev. Biol. *308*, 232–246.

Renström, J., Istvanffy, R., Gauthier, K., Shimono, A., Mages, J., Jardon-Alvarez, A., Kröger, M., Schiemann, M., Busch, D.H., Esposito, I., et al. (2009). Secreted frizzled-related protein 1 extrinsically regulates cycling activity and maintenance of hematopoietic stem cells. Cell Stem Cell *5*, 157–167.

Rőszer, T. (2015). Understanding the Mysterious M2 Macrophage through Activation Markers and Effector Mechanisms. Mediators Inflamm. *2015*, 816460.

Sasmono, R.T., Oceandy, D., Pollard, J.W., Tong, W., Pavli, P., Wainwright, B.J., Ostrowski, M.C., Himes, S.R., and Hume, D.A. (2003). A macrophage colony-stimulating factor receptor-green fluorescent protein transgene is expressed throughout the mononuclear phagocyte system of the mouse. Blood *101*, 1155–1163.

Scott, E.W., Simon, M.C., Anastasi, J., and Singh, H. (1994). Requirement of transcription factor PU.1 in the development of multiple hematopoietic lineages. Science *265*, 1573–1577.

Schmitt, T.M., and Zúñiga-Pflücker, J.C. (2002). Induction of T cell development from hematopoietic progenitor cells by delta-like-1 in vitro. Immunity *17*, 749–756.

Solaimani Kartalaei, P., Yamada-Inagawa, T., Vink, C.S., de Pater, E., van der Linden, R., Marks-Bluth, J., van der Sloot, A., van den Hout, M., Yokomizo, T., van Schaick-Solernó, M.L., et al. (2015). Whole-transcriptome analysis of endothelial to hematopoietic stem cell transition reveals a requirement for Gpr56 in HSC generation. J. Exp. Med. *212*, 93–106.

Spadaro, O., Camell, C.D., Bosurgi, L., Nguyen, K.Y., Youm, Y.H., Rothlin, C.V., and Dixit, V.D. (2017). IGF1 Shapes Macrophage Activation in Response to Immunometabolic Challenge. Cell Rep. *19*, 225–234.

Stremmel, C., Schuchert, R., Wagner, F., Thaler, R., Weinberger, T., Pick, R., Mass, E., Ishikawa-Ankerhold, H.C., Margraf, A., Hutter, S., et al. (2018). Yolk sac macrophage progenitors traffic to the embryo during defined stages of development. Nat. Commun. *9*, 75.

Takahashi, K., Donovan, M.J., Rogers, R.A., and Ezekowitz, R.A. (1998). Distribution of murine mannose receptor expression from early embryogenesis through to adulthood. Cell Tissue Res. *292*, 311–323.

Taoudi, S., and Medvinsky, A. (2007). Functional identification of the hematopoietic stem cell niche in the ventral domain of the embryonic dorsal aorta. Proc. Natl. Acad. Sci. USA *104*, 9399–9403.

Taylor, P.R., Martinez-Pomares, L., Stacey, M., Lin, H.H., Brown, G.D., and Gordon, S. (2005). Macrophage receptors and immune recognition. Annu. Rev. Immunol. *23*, 901–944.

Tober, J., Koniski, A., McGrath, K.E., Vemishetti, R., Emerson, R., de Mesy-Bentley, K.K., Waugh, R., and Palis, J. (2007). The megakaryocyte lineage originates from hemangioblast precursors and is an integral component both of primitive and of definitive hematopoiesis. Blood *109*, 1433–1441.

Travnickova, J., Tran Chau, V., Julien, E., Mateos-Langerak, J., Gonzalez, C., Lelièvre, E., Lutfalla, G., Tavian, M., and Kissa, K. (2015). Primitive macrophages control HSPC mobilization and definitive haematopoiesis. Nat. Commun. *6*, 6227.

Van Gassen, S., Callebaut, B., Van Helden, M.J., Lambrecht, B.N., Demeester, P., Dhaene, T., and Saeys, Y. (2015). FlowSOM: Using self-organizing maps for visualization and interpretation of cytometry data. Cytometry A *87*, 636–645.

Van Rooijen, N., and Sanders, A. (1996). Kupffer cell depletion by liposome-delivered drugs: comparative activity of intracellular clodronate, propamidine, and ethylenediaminetetraacetic acid. Hepatology *23*, 1239–1243.

Wiktor-Jedrzejczak, W.W., Ahmed, A., Szczylik, C., and Skelly, R.R. (1982). Hematological characterization of congenital osteopetrosis in op/op mouse. Possible mechanism for abnormal macrophage differentiation. J. Exp. Med. *156*, 1516–1527.

Yang, Z.F., Poon, R.T., Luo, Y., Cheung, C.K., Ho, D.W., Lo, C.M., and Fan, S.T. (2004). Up-regulation of vascular endothelial growth factor (VEGF) in small-for-size liver grafts enhances macrophage activities through VEGF receptor 2-dependent pathway. J. Immunol. *173*, 2507–2515.

Yokomizo, T., Ng, C.E., Osato, M., and Dzierzak, E. (2011). Three-dimensional imaging of whole midgestation murine embryos shows an intravascular localization for all hematopoietic clusters. Blood *117*, 6132–6134.

Yumine, A., Fraser, S.T., and Sugiyama, D. (2017). Regulation of the embryonic erythropoietic niche: a future perspective. Blood Res. *52*, 10–17.

Zovein, A.C., Hofmann, J.J., Lynch, M., French, W.J., Turlo, K.A., Yang, Y., Becker, M.S., Zanetta, L., Dejana, E., Gasson, J.C., et al. (2008). Fate tracing reveals the endothelial origin of hematopoietic stem cells. Cell Stem Cell *3*, 625–636.

STAR★METHODS

KEY RESOURCES TABLE

REAGENT or RESOURCE	SOURCE	IDENTIFIER
Antibodies		
Anti-Mouse CD41 (MWReg30)-143Nd	Fluidigm	Cat# 3143009C
Anti-Mouse CD45R/B220 (clone RA3-6B2)-144Nd	Fluidigm	Cat# 3144011C
Anti-Mouse CD43 (clone S11)-146Nd	Fluidigm	Cat# 3146009C
Anti-Mouse CD19 (clone 6D5)-149Sm	Fluidigm	Cat# 3149002C
Anti-Mouse CD64 (clone X54-5/7.1)-151Eu	Fluidigm	Cat# 3151012C
Anti-Mouse CD3e (clone 145-2C11)-152Sm	Fluidigm	Cat# 3152004C
Anti-Mouse CD16/32 (clone 93)-153Eu	Fluidigm	Cat# 3153011C
Anti-Mouse F4/80 (clone BM8)-159Tb	Fluidigm	Cat# 3159009C
Anti-Mouse CD11c (clone N418)-162Dy	Fluidigm	Cat# 3162017C
Anti-Mouse CD31/PECAM-1 (clone 390)-165Ho	Fluidigm	Cat# 3165013C
Anti-Mouse Nkp46 (clone 29A1.4)-167Er	Fluidigm	Cat# 3167008C
Anti-Mouse CD206/MMR (clone C068C2)-169Tm	Fluidigm	Cat# 3169021C
Anti-Mouse NK1.1 (clone PK136)-170Er	Fluidigm	Cat# 3170002C
Anti-Mouse CD11b (clone M1/70)-172Yb	Fluidigm	Cat# 3172012C
Anti-Mouse CD117/c-kit (clone 2B8)-173Yb	Fluidigm	Cat# 3173004C
Anti-Mouse I-A/I-E (clone M5/144)-174Yb	Fluidigm	Cat# 3174003C
Anti-Mouse FceR1a (clone MAR-1)-176Yb	Fluidigm	Cat# 3176006C
FITC anti-Mouse/human CD45R/B220 (clone RA3-6B2)	BioLegend	Cat# 103205; RRID: AB_312990
AF647 anti-Mouse CD192 (CCR2) (clone SA203G11)	BioLegend	Cat# 150603; RRID: AB_2566139
PE-Cy7 anti-Mouse CD193 (CCR3) (clone J073E5)	BioLegend	Cat# 144513; RRID: AB_2565739
PE anti-Mouse CD195 (CCR5) (clone HM-CCR5)	BioLegend	Cat# 107005; RRID: AB_313300
BV421 anti-Mouse CD197 (CCR7) (clone 4B12)	BioLegend	Cat# 120119; RRID: AB_10897811
APC/Cy7 anti-Mouse/human CD11b (Mac1) (clone M1/70)	BioLegend	Cat# 101226; RRID: AB_830642
APC anti-Mouse CD206 (mannose receptor) (clone C068C2)	BioLegend	Cat# 141707; RRID: AB_10896057
PE anti-mouse CD3 (clone 17A2)	BioLegend	Cat# 100205; RRID: AB_312662
Alexa Fluor 647 anti-Mouse CD31 (clone MEC13.3)	BioLegend	Cat# 102516; RRID: AB_2161029
BV605 anti-Mouse CD31 (clone 390)	BioLegend	Cat# 102427; RRID: AB_2563982
Anti-Mouse CD34 biotin (clone RAM34)	eBioscience	Cat# 13-0341-82
PE Rat anti-Mouse CD45 (clone 30-F11)	BD Biosciences	Cat# 553081; RRID: AB_394611
BV650 anti-Mouse CD45 (clone 30-F11)	BD Horizon	Cat# 563410; RRID: AB_2738189
APC anti-Mouse CD45.1 (clone A20)	BD Biosciences	Cat# 558701; RRID: AB_1645214
PE anti-Mouse CD45.2 (clone 104)	BD Biosciences	Cat# 560695; RRID: AB_1727493
BV421 anti-Mouse CD117 (c-Kit) (clone 2B8)	BD Biosciences	Cat# 562609; RRID: AB_11154585
BV650 anti-Mouse CX3CR1 (clone SA011E11)	BioLegend	Cat# 149033; RRID: AB_2565999
PerCP-Cy5.5 anti-Mouse CD182 (CXCR2) (clone SA045E1)	BioLegend	Cat# 149605; RRID: AB_2565564
PE Dazzle594 anti-Mouse CD184 (CXCR4) (clone L276F12)	BioLegend	Cat# 146513; RRID: AB_2563682
PE-Cy5 anti-Mouse F4/80 (clone BM8)	eBioscience	Cat# 15-4801-80
PerCP-Cy 5.5 anti-Mouse Flk-1 (clone AVAS12α1)	BD Pharmingen	Cat# 560681; RRID: AB_1727524
Anti-GFP	MBL	Cat# 598; RRID: AB_591819
BV421 anti-Mouse I-A/I-E (clone M5/114.15.2)	BioLegend	Cat# 107631; RRID: AB_10900075

(*Continued on next page*)

Continued

REAGENT or RESOURCE	SOURCE	IDENTIFIER
PE-CF594 anti-Mouse Ly-6C (clone AL-21)	BD Horizon	Cat# 562728; RRID: AB_2737749
AF700 anti-Mouse Ly-6G (clone 1A8)	BD Biosciences	Cat# 561236; RRID: AB_10611860
PE Cy7 anti-Mouse MerTK (clone DS5MMER)	eBioscience	Cat# 25-5751-80
PE anti-Mouse CD202b (Tie2/Tek) (clone TEK4)	eBioscience	Cat# 12-5987
Purified anti-mouse MerTK (clone DS5MMER)	eBioscience	Cat# 14-5751-82
Purified anti-mouse Ly6C (MaxPar ready) (clone HK1.4)	BioLegend	Cat# 128039; RRID: AB_2563783
Purified anti-mouse Ly6G (MaxPar ready) (clone 1A8)	BioLegend	Cat# 127637; RRID: AB_2563784
Purified anti-mouse Siglec F (clone 1RNM44N)	eBioscience	Cat# 14-1702-82
Chemicals, Peptides, and Recombinant Proteins		
Collagenase from Clostridium histolyticum	Sigma-Aldrich	Cat# C0130; Lot# 02M1425V
Critical Commercial Assays		
RNeasy micro kit	Qiagen	Cat# 74004
Deposited Data		
RNA-seq	This paper	GSE130579
Experimental Models: Cell Lines		
Mouse: OP9-DL1	Schmitt and Zúñiga-Pflücker, 2002	Obtained by Prof. Nancy Speck with permission from Zuniga-Plufcker
Mouse: OP9		http://www.lgcstandards-atcc.org/Search_Results.aspx?dsNav=Ntk:PrimarySearch%7cOP9%7c3%7c,Ny:True,Ro:0,N:1000552&searchTerms=OP9&geo_country=gb&redir=1
Experimental Models: Organisms/Strains		
Mouse: B6.Cg-Tg(Csf1r-EGFP)1Hume/J (also known as MacGreen)	The Jackson Laboratory	https://www.jax.org/strain/018549
Mouse: B6.129P2(Cg)-*Cx3cr1*^{tm1Litt}/J (also known as CX3CR1-GFP)	The Jackson Laboratory	https://www.jax.org/strain/005582
Mouse: B6.Cg-Tg(Ly6a-EGFP)G5Dzk/J	The Jackson Laboratory	https://www.jax.org/strain/012643
Mouse: B6.SJL-*Ptprc*^{a}*Pepc*^{b}/BoyCrl (also known as Ly5.1)	Charles River	https://www.criver.com/products-services/find-model/ly51-mouse?region=3671
Oligonucleotides		
See Table S5 for the list of primers		
Software and Algorithms		
FastQC	FastQC: a quality control application for high throughput sequence data	https://www.bioinformatics.babraham.ac.uk/projects/fastqc/
STAR (2.3)	Dobin et al., 2013; STAR: ultrafast universal RNA-seq aligner. Bioinformatics 29, 15–21	https://github.com/alexdobin/STAR
Subread-FeatureCounts (1.5.2)	Liao et al., 2014; FeatureCounts: an efficient general-purpose program for assigning sequence reads to genomic features. Bioinformatics, 30(7):923-30	http://subread.sourceforge.net/
HiSat (2.0.4)		https://ccb.jhu.edu/software/hisat2/index.shtml
Prism Version 5	GraphPad	http://www.graphpad.com/scientific-software/prism
BD Facs Diva version 8	BD Biosciences	http://www.bdbiosciences.com/en-us
Image J	NIH	https://imagej.nih.gov/ij/
Slidebook 6	3i	https://www.intelligent-imaging.com/slidebook
FlowJo Version 8.7 and 10.1r5	Tree Star, Inc	https://www.flowjo.com/solutions/flowjo/downloads/previous-versions

(*Continued on next page*)

Continued

REAGENT or RESOURCE	SOURCE	IDENTIFIER
MATLAB Version 2013b		N/A
FlowSOM	Cytobank, Inc	https://premium.cytobank.org/cytobank/
Other		
R coding for CyTOF analysis	This paper	https://github.com/markrobinsonuzh/samanta_cytof_analysis_code

CONTACT FOR REAGENT AND RESOURCE SHARING

Further information and requests for resources and reagents should be directed to and will be fulfilled by the Lead Contact, Elaine Dzierzak (elaine.dzierzak@ed.ac.uk).

EXPERIMENTAL MODEL AND SUBJECT DETAILS

All mice were housed and bred in animal facilities at the University of Edinburgh, in compliance with the Home Office regulations. All procedures with animals were conducted by a Home Office UK Project License (PPL 70/8076) and approved by the University of Edinburgh Ethical Review Committee.

METHOD DETAILS

Mouse and embryo generation

Wild type C57BL/6 from animal facility of the University of Edinburgh, *MacGreen (*B6.Cg-Tg(Csf1r-EGFP)1Hume/J) (Sasmono et al., 2003), *Cx3cr1-GFP* (B6.129P2(Cg)-*Cx3cr1*^{tm1Litt}/J)(Jung et al., 2000) and *Ly6aGFP* (B6.Cg-Tg(Ly6a-EGFP)G5Dzk/J) (de Bruijn et al., 2002) mice were used for timed mating. Embryos were generated from *MacGreen* (mixed background backcrossed six times into C57BL/6HsdJOla) and *Ly6aGFP* (C57BL/6HsdJOla background) males (two to eight months old) crossed with wild type female mice (two to six months old) and *Cx3cr1*$^{gfp/wt}$ males (two to eight months old, mixed background backcrossed five times into C57BL/6HsdJOla) crossed with *Cx3cr1*$^{gfp/wt}$ females (two to six months old). Accurate embryo staging was done by somite pair counts. Ly5.1 mice (B6.SJL-*Ptprc*^{a}*Pepc*^{b}/BoyCrl, two to four months old) were used as recipients of transplantation experiments.

Mass cytometry (CyTOF)

Mass cytometry antibodies were either labeled in-house by using antibody-labeling kits (Fluidigm, California, USA) or purchased (Fluidigm). Antibodies were individually titrated and optimized prior to use. Six palladium metal isotopes were used for live cell barcoding of samples with CD45 (Mei et al., 2015), while keeping CD45-89Y as a common channel to clearly identify cells expressing varying degrees of CD45. Briefly, individual samples from YS, AGM and adult C57BL/6 mouse spleens were incubated with respective CD45-Pd + antibodies in PBS for 30min at room temperature, washed twice with FACS buffer (PBS supplemented with 0.5% BSA), and then pooled into one sample. This was followed by incubation of samples with the cocktail of primary panel antibodies (SuppTable1 and KRT) for 20 min at room temperature and washing with FACS buffer. After washing, samples were incubated with intercalating solution (Iridium in MaxPar Fix/Perm buffer (both Fluidigm)) overnight at 4^{o} C. Prior to acquisition, the samples were washed twice with MilliQ water. Barcoded composite samples were acquired on a Helios mass cytometer (Fluidigm). Quality control and tuning processes on the Helios were performed on a daily basis before acquisition. Data from different days and across acquisition time was normalized by adding five-element beads to the sample immediately before acquisition and using the MATLAB-based normalization software (Version 2013b) (Finck et al., 2013).

Mass cytometry statistical analysis

Live cells were exported by manual gating on Event_length, DNA (191Ir and 193Ir), CD45-89Y, and live cells (198Pt) using FlowJo software (Version10.1r5, Tree Star) (Krieg et al., 2018). For further analysis, we used our customized R workflow (Nowicka et al., 2017). All analyses on CyTOF data were performed after arcsinh (with base equal to 5) transformation of marker expression. In brief, pre-processing of the raw data was followed by dimensionality reduction and visualization by t-Distributed Stochastic Neighbor Embedding (t-SNE) with parameters as listed in the figure legends, clustering with FlowSOM into initial 100 nodes (Van Gassen et al., 2015), followed by expert-guided manual metaclustering.

Whole-mount Images

MacGreen embryos were fixed in 2% PFA-PBS for 20min and dehydrated in 50% methanol in PBS for 10 min followed by 100% methanol for 2x10min. The body wall was trimmed on both sides of the embryo, exposing the AGM for immunochemistry. Embryos were then rehydrated in 50% methanol in PBS (Sigma-Aldrich, Missouri, USA) for 10 min following by PBS and incubated overnight at 4°C with rabbit anti-GFP (1:1000; MBL International, Massachussetts, USA) and rat anti-c-Kit (1:500; eBioscience, Thermo Fisher

Scientific, Massachussetts, USA). At 4°C, embryos were washed in PBS-MT (PBS supplemented with 1% skim milk (BioRad, California, USA) and 0.4% TritonX-100 (Acros Organics, Thermo Fisher Scientific) for 3x2hr and incubated overnight with anti-rabbit AlexaFluor488 (1:1000; Invitrogen) and anti-rat AlexaFluor647 (1:5000; Invitrogen, Thermo Fisher Scientific), then washed in PBS-MT for 3x2hr and incubated overnight with biotinylated rat anti-CD31 (1:500; BD Biosciences, New Jersey, USA), then washed in PBS-MT for 3x2hr and incubated overnight with Streptavidin AlexaFluor555 (1:500; Invitrogen, Thermo Fisher Scientific). Embryos were then washed in PBS supplemented with 0.4% TritonX-100 (PBST) and mounted in a FastWell (Sigma-Aldrich) for imaging using a Leica SP5 confocal microscope. Using Fiji (ImageJ), a maximum projection image with merged colour channels was generated.

Tissue Sections

MacGreen embryos were fixed in 2% PFA-PBS for 30 mins and washed in PBS for 10 mins at 4°C. Embryos were then equilibrated in 20% sucrose in PBS for 30 mins at 4°C. Embryos were washed in OCT embedding matrix for frozen sections (CellPath, Thermo Fisher Scientific), using tissue paper to remove remaining sucrose. Each embryo was placed in an individual mould containing OCT and orientated forelimbs exactly above hindlimbs and YS to one side before being quickly frozen on dry ice in absolute ethanol. Frozen OCT blocks were then removed from the mould, wrapped in Parafilm^{R} and stored at -80°C. 10μm sections were taken along the length of the AGM of MacGreen embryos using a Bright OTF5000 cryostat and placed on poly-lysinated glass slides (Thermo Fisher Scientific) 8 sections/slide that were then stored at -20°C. For immunohistochemistry, slides were blocked in 50% Avidin D solution (Vector Laboratories Inc., California, USA) diluted in PBS supplemented with 0.05% Tween20 and 1% bovine serum albumin (BSA) (PBS_{block}) and washed in PBST. Slides were incubated for 1hr with rat anti-CD34 (1:200; eBioscience, Thermo Fisher Scientific), rabbit anti-GFP (1:1000; MBL International) and rat anti-CD206 (MR; 1:50; BioLegend, California, USA) diluted in PBS_{block} at RT and washed in PBST, then incubated for 1hr with anti-rabbit AlexaFluor488 (1:1000; Invitrogen, Thermo Fisher Scientific) and Streptavidin Cy3 (1:2500; Jackson ImmunoResearch Laboratories, Pennsylvania, USA)) diluted in PBS_{block} at RT and washed in PBST before 10mins incubation in DAPI (1:1000) diluted in PBS_{block} at RT. Slides were washed and mounted with coverslips using SlowFade Diamond Anti-Fade Mountant (Invitrogen, Thermo Fisher Scientific). Sections were imaged on a Leica SP5 confocal microscope. 10 sections from along the length of the AGM were imaged per embryo. Using Fiji (ImageJ), a maximum projection image of each section with merged colour channels was obtained.

Time-lapse *ex vivo* imaging

MacGreen embryos were stained by intra-aortic flushing with anti-CD31-AF647 (clone MEC13.3, Biolegend) and anti-c-Kit-BV421 (clone 2B8, BD Biosciences) antibodies and incubated 30min at 4°C in PBS + 10% FBS. The embryos were then transversally thick-sectioned with an automatic tissue chopper into 150μm sections that were embedded in low melting agarose (Sigma-Aldrich) and placed in a chamber ring support (Attofluor cell chamber, Invitrogen, Thermo Fisher Scientific) closed at the bottom with a round glass cover slip (Menzel Gläser, VWR, Pennsylvania, USA). The agarose-embedded sections were then covered with MyeloCult M5300 medium (StemCell Technologies) supplemented with hydrocortisone succinate 10^{-6}M (Sigma-Aldrich) and mIL3 20ng/ml (Peprotech, New Jersey, USA). Overnight imaging was performed either on a CSU-W1 Spinning disk confocal (Videos S1 and S2) or a Andor spinning disk (20x objective) and analyzed with the integrated software with a 10-minute interval for a total of 14–16 h, step size 3 μm and a z-range of 20–40 steps. The samples were maintained at 37°C. Videos were analyzed with Slidebook software (3i, Colorado, USA). Lateral drifting of the section imaged in the movie 2 was corrected with Huygens software.

AGM explant cultures

AGM from E10.5 MacGreen embryos (34-39sp) were dissected and cultured for 72 h at 37° C with 5% CO_2 at the air-liquid interface in a six well plate on a metal mesh covered with durapore membrane filter paper (Millipore, Massachusetts, USA). The MyeloCult M5300 medium (StemCell Technologies) used was supplemented with hydrocortisone succinate 10^{-6}M (Sigma-Aldrich).

CFU-C assay and stem cell transplantation

Cells from AGM or AGM explants were digested at 37°C in 0.125% type 1 collagenase (C0130, Sigma- Aldrich) for 45 min and then cultured in Methylcellulose (M3434; Stem Cell Technologies, Canada) at 37° C with 5% CO_2. Colonies were counted and scored after 10 days.

AGM explant cells were prepared into single cell suspensions, as described above, and injected intravenously into irradiated Ly5.1 recipients two doses of 4.5 Gy of γ-irradiation). After 4 and 16 weeks, peripheral blood was taken for CD45.1- and CD45.2- flow cytometric analysis. Recipient mice are considered reconstituted when ≥5% of cells are donor-derived.

OP9/OP9-DL1 co-culture system

AGM derived endothelial cells ($CD31^{+}CD45^{-}CD41^{-}$) and macrophages ($CD206^{+}$ and $CD206^{-}$) were co-cultured with OP9-DL1 cells at 37° C with 5% CO_2 in cytokine containing αMEM (SCF100ng/ml, IL3 100ng/ml and Flt3-ligand 100ng/ml, Peprotech). After seven days of co-culture, $CD45^{+}$ cells were FACS sorted and plated in methylcellulose (M3434; Stem Cell Technologies). Colonies were counted and scored after 10 days. For the transwell experiment, Corning HST Transwell (Thermo Fisher Scientific) with 3μM pores were used to separate the endothelial cells (bottom of the well) from macrophages. $CD206^{+}$ macrophages were put either in contact with endothelial cells or at the top of the transwell filter. After 7 days of co-culture, at 37° C with 5% CO_2, $CD45^{+}$ cells derived from the endothelial cells (bottom of the transwell) were FACS sorted and plated in methylcellulose. Colonies were counted and scored after

10 days. For the lymphoid potential progenitor assay, AGM explants were digested and single cells plated on OP9 stromal cells in αMEM with the addition of IL7 20ng/ml and Flt3 20ng/ml. Medium was replaced every 3 days and the cells were plated on fresh OP9 every 7 days. Flow cytometric analysis for macrophage and B cell markers was performed after 10 days of co-culture.

BLZ945 and Clodronate-liposome treatment

AGM explants were pre-incubated for 2 h at 37°C in MyeloCult M5300 medium + BLZ945 (0.67, 6.7 or 67 μM) or clodronate-liposomes (1:5 dilution) and their controls, DMSO and PBS-liposomes, respectively. Then the explants were recovered from the wells with curved forceps and placed for 72 h on the metal mesh + filter paper (see above for details). The treatments were added to the explant medium at time zero and 48 h later.

Flow analysis and sorting

Cells from AGM, YS, culture systems and hematopoietic organs of adult mice were blocked in PBS+10%FBS and then stained with antibodies (SupTable4) for 30 min on ice. Excess of antibodies was washed away with PBS/FBS before flow cytometry analysis. Sorted cells were collected in 50% PBS/FBS for functional analyses or in Qiagen RLT lysis buffer for RNA extraction. Cytometry was performed on LSR Fortessa, AriaII and Fusion (BD Bioscience).

Gene Expression Analysis

RNA from sorted cells was extracted by using RNeasy Micro Kit (Qiagen, Germany). cDNAs were generated using oligdT primers and SuperScript III Reverse Transcriptase (Invitrogen Thermo Fisher Scientific) according to manufacturer instructions. RT-PCR were performed by using Fast SYBR Green Master Mix (Thermo Fisher Scientific) on an ABI 7900 machine (Applied Biosystems, California, USA). See Table S5 for the list of the primers used.

RNA-seq

RNA from sorted cells (*MacGreen* GFP^+CD206^- and GFP^+CD206^-) was extracted by using RNeasy Micro Kit (Qiagen) and the RNASeq samples were prepped according to the Smart-seq2 method (Picelli et al., 2013). The samples were then sequenced according to the Illumina TruSeq Rapid v2 protocol on the HiSeq2500 machine with a single read 51 bp and dual 9+9bp index and mapped against the requested reference using HiSat2 (version 2.0.4). Gene expression values were called using htseq-count (version 0.6.1).

Sequencing alignment and Quantification

Fastq files of 51bp single-end reads were quality controlled using FASTQC. Reads were then aligned to the GENCODE M14 mouse reference genome (mm10) using STAR aligner (version 2.3) for Linux Ubuntu, with default options, and ran over 8 threads per sample. For improved accuracy, the exon junction coordinates from the reference annotation were used. Resulting BAM files from different lanes were merged into one sample. Gene quantification on the merged samples was performed using featureCounts from the subRead package.

Statistical analysis for differentially expressed genes

All statistical calculations have been performed in R programming language (version 3.2.3). Genes with expression 0 or 1 were filtered out. Differential expression analysis was performed using DESeq2 package to identify significantly differentially expressed genes with controlled False Positive Rate (B&H method) at 5% (FDR $\leq$ 0.05). Up-regulated genes were selected at a minimum $\log_2$ fold change of 1.5 and down-regulated genes at a minimum $\log_2$ fold change of -1.5. Principle component analysis was performed on the regularized log transformed (rlog) expression matrix on all genes. Heatmaps were drawn on the regularized transformed (rlog) expression matrix (*pheatmap* package). Pearson correlation and average linkage were used for hierarchical clustering.

QUANTIFICATION AND STATISTICAL ANALYSIS

All graphs were generated using GraphPad Prism 5. A one-way Anova with Dunnett post-hoc test was used to compare total macrophages numbers in the AGM to that in the non-AGM region. To compare tissue section cell counts for GFP^+CD206^- and GFP^+CD206^+ macrophages across the different regions, a two-way ANOVA with multiple comparisons corrected by a Tukey's range test was used. A one-way ANOVA corrected by Bonferroni's test was used to compare more than 2 groups, whereas the Student's t test was used when the groups to compare were only two. Details of the statistical test used can be found in the figure legends. Significance was defined as $p < 0.05$. *$p < 0.05$, **$p < 0.01$, ***$p < 0.001$.

DATA AND SOFTWARE AVAILABILITY

The accession number for the RNA-seq data reported in this paper is GSE130579.